Hindawi
Geofluids
Volume 2022, Article ID 3399984, 23 pages
https://doi.org/10.1155/2022/3399984

Research Article

Overlying Rock Activity Laws and Influential Ranges of Coal Seam Mining in Stubble Areas

Baoxin Jia,[1] Hao Chen,[1] Zhiyong Li,[1,2] and Zhi Tang[3]

[1]*School of Civil Engineering, Liaoning Technical University, Fuxin 123000, China*
[2]*China Construction Eighth Engineering Bureau, Jinan 250100, China*
[3]*School of Mechanics and Engineering, Liaoning Technical University, Fuxin 123000, China*

Correspondence should be addressed to Hao Chen; 1041336882@qq.com

Received 7 January 2022; Accepted 14 March 2022; Published 16 April 2022

Academic Editor: Xuelong Li

This report applies theoretical analysis, similar material simulations, and numerical simulation methods to study the overburden strata movements and influential range of coal mining under pressure stubble conditions and to elucidate the relationship between adjacent coal seams. The pressure, failure, caving, stress, and displacement of crop conditions during coal seam mining were evaluated. The results show that the overlying $W_{9\text{-}10}$ coal face and underlying $J_{16\text{-}17}$ roof experience a long first pressure step, i.e., close to the periodic weighting distance. The working face of the $W_{9\text{-}10}$ coal seam is located in the bending subsidence zone of the working face of the $J_{16\text{-}17}$ coal seam. With the advance of the working face of the $J_{16\text{-}17}$ coal seam, the development and range of overburden fracture of the $W_{9\text{-}10}$ coal seam gradually increase. The supporting pressure and displacement caused by the mining process at the W coal seam have no impact on the coal seam of the stubble area, whereas the mining of the J coal seam leads to a continuous increase in the overburden displacement of the W coal seam; the latter also induces a shift in the maximum displacement to the rear, which is more significant for the stress concentration at the middle and front regions of the stubble area, thus presenting a superposition effect. The stress caused by mining at the coal seam decreases with increasing vertical distance from the roof or floor. For distant coal seams, the main contributing factor is the effect of vertical stress. The influential range of the vertical stress caused by mining in the overlying working face remains within 90 m, whereas the influential range of the stress caused by mining in the underlying working face is relatively large, i.e., it still affects the roadway at distances up to 160 m. The results and discussion presented herein provide significant practical value in terms of understanding the overburden strata activity and its influential range in adjacent mines' stubble areas, which can be used to guide group mining efforts.

1. Introduction

Coal resources have long served as the main energy source in China; mining is often accompanied by the occurrence of dynamic hazards such as impact ground pressure [1, 2] and coal and gas protrusion [3], and safe mining becomes particularly important [4, 5], and continuous research and developments have gradually improved the technology used to mine mineral resources. The influence of coal seam mining (between adjacent mines) on the deformation and failure of the rock surrounding roadways has also emerged as a prominent area of interest. Most mining areas encounter coal seam mining problems with adjacent mines (e.g., in the Datong and Pingdingshan mining areas), where the occurrence and recoverable amounts are large. Therefore, it is urgently crucial to elucidate the impacts of adjacent coal seam mining to ensure safe production and sustainable development.

Currently, the mining of multilevel coal seams [6, 7] causes various phenomena and influences the range of mining, pressure release, fracture development, and rock strata movement. Guo et al. [8, 9] used photoelastic mechanical model analysis and simulation experiments to investigate the simultaneous mining of multiple coal seams; they determined the coal seam relationships, stress distributions, and strata behavioral characteristics of multiple coal seam

mining, which provided a basis for studying the stress factors influencing multiple coal seam mining. Yang et al. [10] used a combination of mechanical analysis and numerical simulation to investigate the stress distribution pattern and damage characteristics of the bottom slab. Through theoretical analysis and laboratory simulations, Shi [11, 12] established the stress law of coal seam floor strata under coal seam mining conditions. Lu and coworkers [13, 14] summarized a large amount of data and clarified the influence of upper coal seam mining on the underlying vertical distance and surrounding rock lithology. On this basis, the relationships among various factors affecting the vertical distance were deduced, and importantly, the relationship between the horizontal spacing of coal pillars in a roadway and the spacing of overlying coal seams was obtained. Luo and Yang [15] used similar material simulation experiments to analyze the existing law of mine pressure at the coal seam mining face, as well as its influence on the roadway, thereby provided a reference for other coal seam roadway layouts involving proximal coal seams. Yang et al. [16] investigated the spatial and temporal evolution characteristics of repeated mining overburden fractures in close coal seams under upward and downward mining methods using similar material model tests. Yue et al. [17] constructed a structural mechanics model of "elliptical stress arch" of the overlying coal seam; numerically simulated the morphological parameters of the "elliptical stress arch," such as the coordinates of the center of the circle, the length of the axis, and the position of the foot of the arch; determined the width of each area of the base plate of the overlying coal seam and its equivalent load; and calculated the additional stress in the roadway of the base plate of the underlying coal seam. Liu et al. [18] established a nonuniform superimposed stress model for coal pillars from the energy accumulation and release of the surface roadway envelope after the destruction of coal pillars according to the engineering geological conditions of a mine in order to reveal the instability of the roadway envelope. Liu [19] applied theoretical analysis and field monitoring techniques to determine the influential range and degree of abutment pressure caused by mining at the working face of the roadway floor while considering the influence of the overlying coal seam mining on the deformation and failure law of the rock surrounding the roadway floor. Zhao et al. [20] studied the impacts of coal seam mining on the roadway floor via theoretical analysis and numerical simulations. They concluded that the instability of the surrounding rock of the roadway floor was a result of the transfer of the mining stress of the overlying coal seam along the floor direction. Guo and Li [21] employed theoretical analysis and numerical simulations to analyze the effects of long-distance lower coal seam mining on the overlying roadway. It was determined that the deformation and failure of the overlying roadway were induced by the overlying strata damage and movement caused by mining at the underlying working face. Zhao et al. [22] obtained the stress and fracture evolution law of the surrounding rock in close coal seam stirrup mining by combining theoretical calculation, numerical simulation, and field measurement. Zhou et al. [23] used the UDEC numerical simulation software to model the roof roadway during the upward mining of the coal seam. Their analysis indicated that the main form of deformation of the roof roadway surrounding rock under the influence of mining was the deformation of the roof and floor of the roadway, followed by the deformation near the side of the working face. Simultaneously, as the advancing distance of the working face increased, the development of mining-induced cracks and plastic zones in the surrounding rock of the stope and the roadway constantly promoted one another.

To date, research advancements in single coal seam and close coal seam mining have made significant contributions to the safe and effective operation of coal mines. However, there are few studies investigating the influence of coal seam mining on the deformation law of roadway surrounding rock under conditions involving stubble. The relationships among coal seam stubble in adjacent mines, pressure release, fracture development, rock strata movement, and other laws impacted by coal seam mining have unique properties within the scope of influence, which make it more difficult to control the roadway surrounding rock during coal seam mining [24–28]. Therefore, it is necessary to evaluate the variation law, influential range, and deformation law of surrounding rock in terms of the mining-induced stress of the stubble coal seam. Therefore, this report discusses the laws governing overburden caving, the stress and displacement changes, and the influential range of coal seam mining in stubble environments based on the relationship between the No. 5 and No. 6 coal seams of the Pingdingshan Coal Mine. According to the theory of elasticity mechanics, the stress field calculation model of overburden working face and underburden working face of stubble coal seam is established, and the expression of stress caused by mining of working face is derived, and the change law of vertical stress, horizontal stress, and shear stress in top and bottom plate with vertical distance is analyzed according to engineering geological conditions, similar material simulation experiments, and numerical simulation, and the overburden rock collapse, the stress and displacement change law, and the influence range of coal seam mining under stubble environment are revealed.

2. Theoretical Calculations of Coal Seam Mining in Stubble Area

2.1. Overview of Adjacent Mine Stubble Working Face. The Pingmei No. 6 coal mine is considered a large mine because it has an annual output of over 3 million tons. The No. 5 coal mine is located through the Guodishan fault at the southwest end of the bottom of the No. 6 coal mine. Because of resource depletion, the original mine (No. 5 coal mine) underwent a technical transformation in 1998 to prolong the service life of the mine. According to the Pingmei Group, this transformation specifically involved the expansion of the J coal group, such that the boundary of the J coal section of the No. 5 coal mine was expanded to the original J coal seam of the No. 6 coal mine. Following approval from the Ministry of Land and Resources in 2001, the mining permit

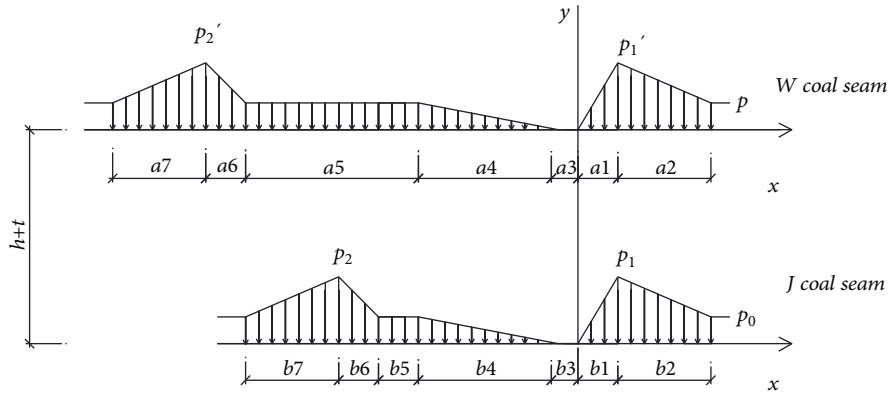

Figure 1: Mechanical model of underground structure.

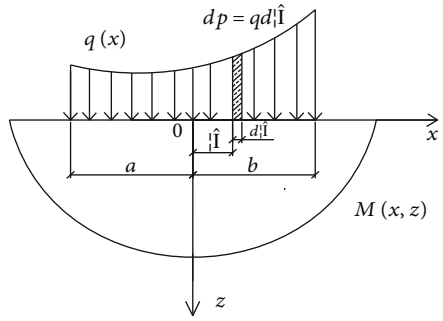

Figure 2: Half infinite plane load distribution.

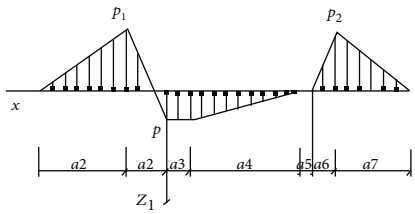

Figure 3: Distribution diagram of additional stress in the floor after mining at the W coal seam.

was replaced. Thus, there is a stubble relationship between the coal seams in the No. 5 and No. 6 coal mines.

The pseudo-top lithology of the $W_{9\text{-}10}$ coal seam in the No. 6 coal mine includes sandy mudstone or mudstone, with thickness of approximately 0.2–0.6 m. The direct roof lithology is mudstone or fine- to medium-grained sandstone, and the old roof lithology is fine- to medium-grained sandstone with a thickness of approximately 6–8 m. The floor lithology is sandy mudstone with a thickness of ~10 m; the $W_{9\text{-}10}$ coal seam thickness is between 0.62 and 7.65 m, with an average thickness of 3.80 m. The coal body is massive; within the scope of the mine field, the recoverable index of the $W_{9\text{–}10}$ coal seam is km = 0.96, which indicates that it is a relatively stable coal seam. In this paper, the thickness of coal seam is taken as 4 m.

The No. 5 mine has a $J_{16\text{-}17}$ coal seam position in the No. 6 mine $W_{9\text{-}10}$ coal seam below the average distance of 160 m. Some areas have a pseudo-top lithology of carbonaceous mudstone with a thickness of approximately 0.2–0.5 m. The direct roof lithology is mudstone and fine-grained sandstone (thickness = ~ 10 m), and the lithology of the old roof is fine- to medium-grained sandstone (thickness = 5 – 8 m). The coal body of coal seam $J_{16\text{–}17}$ in the No. 5 coal mine is mostly block-like and granular, which comprise a coal seam with a simple structure. The thickness of this layer is approximately 0.61–17.5 m, and the average thickness is 5.12 m. The thickness of this coal seam is 5 m.

To study the variation and distribution of mining stress caused by coal seam mining, it is necessary to analyze and study the No. 6 mine W coal seam floor and the No. 5 coal mine J coal seam roof. According to the site construction environment and mining sequence, the No. 6 mine's W coal seam was mined first, followed by the mining of the No. 5 mine's J coal seam.

The propagation of support pressure caused by coal seam mining along the roof and floor will impact the adjacent coal seams. Therefore, the concept of well groups is proposed. A so-called well group is directly related to the spacing between two or more mines, i.e., the spacing between mines determines the impact of mining one coal seam on one or more additional coal seams. The propagation of support pressure along the roof and floor caused by coal seam mining adopts a certain range. Thus, it is crucial to study the influential range and law of mining stress in adjacent coal seams to reveal the mechanism of dynamic disasters affecting a well group. In this work, the variation and distribution law of mining-induced stress in rock mass were analyzed as a function of the vertical distance during coal seam mining in two adjacent mines. The stubble-pressing diagram was constructed based on the stubble-pressing relationship between the No. 5 and No. 6 mines in the Pingdingshan Coal Mine. The floor strata after coal seam excavation are regarded as a spatial semi-infinite body. A vertical section is taken along the direction of coal seam advancement, and the thickness is taken as the unit thickness. A simplified mechanical model of the underground structure of the stubble-pressing coal seam in adjacent mines is established, as shown in Figure 1.

According to the elastic mechanics, when the load is $q(x)$ at the boundary of the homogeneous isotropic semi-infinite

plane, the resulting load distribution is illustrated in Figure 2.

To compute the stress at a point $M(x, z)$ in the half plane, the micro element $d\xi$ is determined at a distance from the origin ξ, and the force on this element $dp = qd\xi$ is taken as the micro-concentrated force. Then, the coordinate of point M relative to the micro-concentrated force is $(x - \xi, z)$. According to the principles of elastic mechanics, the stress at any point M in this plane can be expressed as shown in Equation (1), where σ_z is the vertical stress, σ_x is the horizontal stress, and τ_{xz} is the shear stress.

$$\left.\begin{aligned}\sigma_z &= \frac{2}{\pi}\int_{-a}^{\mathrm{b}} \frac{qz^3}{\left[(x-\xi)^2+z^2\right]^2}d\xi \\ \sigma_x &= \frac{2}{\pi}\int_{-a}^{b} \frac{qz(x-\xi)^2}{\left[(x-\xi)^2+z^2\right]^2}d\xi \\ \tau_{xz} &= \frac{2}{\pi}\int_{-a}^{b} \frac{qz^2(x-\xi)}{\left[(x-\xi)^2+z^2\right]^2}d\xi\end{aligned}\right\}. \tag{1}$$

2.2. Stress Distribution Law of the W Coal Seam Mining Floor in the No. 6 Coal Mine. The influence of the W coal seam on the floor strata in the No. 6 coal mine was analyzed to evaluate the stress state. Considering the stress distribution caused by coal seam mining and the integrity of propagation, the influence of fixed support pressure was introduced to the previous model. The stress change caused by coal seam excavation can be expressed in the form of additional stress. The additional stress value is the difference between the stress of the coal seam floor and the stress of the original rock. Thus, the complete additional stress distribution law of the floor after the mining of the coal seam was obtained, as shown in Figure 3.

Herein, p represents the additional stress in the goaf; p_1 is the maximum additional stress value in front of the coal wall, such that $p_1 = (k_1 - 1)\gamma H$; p_2 is the maximum additional stress behind the opening, such that $p_2 = (k_2 - 1)\gamma H$; a_1 is the spacing between the coal wall and the peak pressure ahead; a_2 is the spacing between the peak pressure ahead and the stress descending to the original rock; a_3 is the distance from zero stress in the original rock in the mined-out area; a_4 is the restoration of residual pressure in the goaf relative to the original rock stress spacing; a_5 is the distance from the restoration to the original rock stress; a_6 is the distance between the peak abutment pressure and the open cut; a_7 is the distance between the peak pressure and the stress falling to the original rock. According to Figure 3, the linear function of the additional stress on the floor of the W coal seam can be expressed as

$$q(x) = \begin{cases} \dfrac{p_1 + p}{a_1}x - p & x \in (0, a_1) \\ -\dfrac{p_1}{a_2}x + \dfrac{(a_1 + a_2)p_1}{\mathrm{a}_2} & x \in (a_1, a_1 + a_2) \\ -p & x \in (-a_3, 0) \\ -\dfrac{p}{a_4}x - \dfrac{p(a_3 + a_4)}{a_4} & x \in (-a_3 - a_4, -a_3) \\ -\dfrac{p_2}{a_6}x - \dfrac{(a_3 + a_4 + a_5)p_2}{a_6} & x \in (-a_3 - a_4 - a_5 - a_6, -a_3 - a_4 - a_5) \\ \dfrac{p_2}{a_7}x + \dfrac{(a_3 + a_4 + a_5 + a_6 + a_7)p_2}{a_7} & x \in (-a_3 - a_4 - a_5 - a_6 - a_7, -a_3 - a_4 - a_5 - a_6) \end{cases}. \tag{2}$$

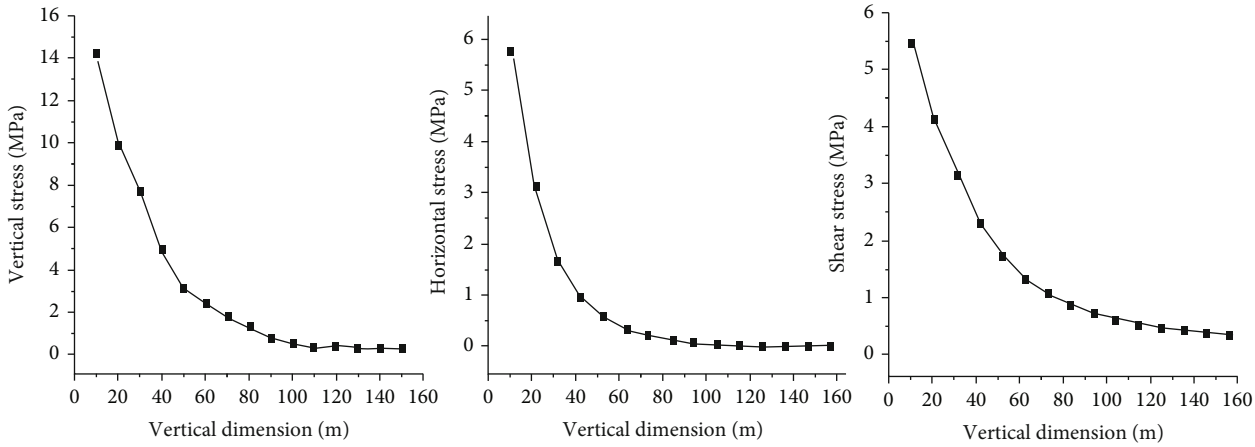

Figure 4: Variations in the floor stress components of the W coal seam as a function of the vertical distance.

The additional stress at a point in the lower area of the floor during the mining process of the coal seam can be obtained using Equations (1) and (2). The additional vertical stress, shear stress, and horizontal stress are expressed as

$$\begin{aligned}\sigma_{z_1} = {} & \frac{2}{\pi}\int_{-a_3-a_4-a_5-a_6}^{-a_3-a_4-a_5-a_6-a_7} -\frac{p_2(x+a_3+a_4+a_5+a_6+a_7)}{a_7}\frac{z^3}{\left[(x-\xi)^2+z^2\right]^2}d\xi \\ & + \frac{2}{\pi}\int_{-a_3-a_4-a_5}^{-a_3-a_4-a_5-a_6}\frac{p_2(x+a_3+a_4+a_5)}{a_6}\frac{z^3}{\left[(x-\xi)^2+z^2\right]^2}d\xi \\ & + \frac{2}{\pi}\int_{-a_3-a_4}^{-a_3}\frac{p(x+a_3+a_4)}{a_4}\frac{z^3}{\left[(x-\xi)^2+z^2\right]^2}d\xi + \frac{2}{\pi}\int_{-a_3}^{0} \mathrm{p}\frac{z^3}{\left[(x-\xi)^2+z^2\right]^2}d\xi \\ & + \frac{2}{\pi}\int_{0}^{a_1}\left(-\frac{p_1+p}{a_1}x+p\right)\frac{z^3}{\left[(x-\xi)^2+z^2\right]^2}d\xi \\ & + \frac{2}{\pi}\int_{a_1}^{a_1+a_2}\frac{p_1(x-a_1-a_2)}{a_2}\frac{z^3}{\left[(x-\xi)^2+z^2\right]^2}d\xi,\end{aligned} \tag{3}$$

$$\begin{aligned}\sigma_{x_1} = {} & \frac{2}{\pi}\int_{-a_3-a_4-a_5-a_6}^{-a_3-a_4-a_5-a_6-a_7} -\frac{p_2(x+a_3+a_4+a_5+a_6+a_7)}{a_7}\frac{z(x-\xi)^2}{\left[(x-\xi)^2+z^2\right]^2}d\xi \\ & + \frac{2}{\pi}\int_{-a_3-a_4-a_5}^{-a_3-a_4-a_5-a_6}\frac{p_2(x+a_3+a_4+a_5)}{a_6}\frac{z(x-\xi)^2}{\left[(x-\xi)^2+z^2\right]^2}d\xi \\ & + \frac{2}{\pi}\int_{-a_3-a_4}^{-a_3}\frac{p(x+a_3+a_4)}{a_4}\frac{z(x-\xi)^2}{\left[(x-\xi)^2+z^2\right]^2}d\xi + \frac{2}{\pi}\int_{-a_3}^{0} \mathrm{p}\frac{z(x-\xi)^2}{\left[(x-\xi)^2+z^2\right]^2}d\xi \\ & + \frac{2}{\pi}\int_{0}^{a_1}\left(-\frac{p_1+p}{a_1}x+p\right)\frac{z(x-\xi)^2}{\left[(x-\xi)^2+z^2\right]^2}d\xi \\ & + \frac{2}{\pi}\int_{a_1}^{a_1+a_2}\frac{p_1(x-a_1-a_2)}{a_2}\frac{z(x-\xi)^2}{\left[(x-\xi)^2+z^2\right]^2}d\xi,\end{aligned} \tag{4}$$

$$\begin{aligned}\tau_{xz_1} = {} & \frac{2}{\pi}\int_{-a_3-a_4-a_5-a_6}^{-a_3-a_4-a_5-a_6-a_7} -\frac{p_2(x+a_3+a_4+a_5+a_6+a_7)}{a_7}\frac{z^2(x-\xi)}{\left[(x-\xi)^2+z^2\right]^2}d\xi \\ & + \frac{2}{\pi}\int_{-a_3-a_4-a_5}^{-a_3-a_4-a_5-a_6}\frac{p_2(x+a_3+a_4+a_5)}{a_6}\frac{z^2(x-\xi)}{\left[(x-\xi)^2+z^2\right]^2}d\xi \\ & + \frac{2}{\pi}\int_{-a_3-a_4}^{-a_3}\frac{p(x+a_3+a_4)}{a_4}\frac{z^2(x-\xi)}{\left[(x-\xi)^2+z^2\right]^2}d\xi + \frac{2}{\pi}\int_{-a_3}^{0} \mathrm{p}\frac{z^2(x-\xi)}{\left[(x-\xi)^2+z^2\right]^2}d\xi \\ & + \frac{2}{\pi}\int_{0}^{a_1}\left(-\frac{p_1+p}{a_1}x+p\right)\frac{z^2(x-\xi)}{\left[(x-\xi)^2+z^2\right]^2}d\xi \\ & + \frac{2}{\pi}\int_{a_1}^{a_1+a_2}\frac{p_1(x-a_1-a_2)}{a_2}\frac{z^2(x-\xi)}{\left[(x-\xi)^2+z^2\right]^2}d\xi.\end{aligned} \tag{5}$$

According to Equations ((3)–(5)), after mining at the working face of the W coal seam, the spatial position and load bearing condition of a point under the floor determine the stress at this point. In a practical situation, the current load is a known quantity, and therefore, the stress value is a function of (x, z). According to the technical conditions and field observations, the average bulk density of the overburden γ is 0.025 MPa, the thickness of the overburden is 714 m, the stress of the original rock is $p = -\gamma h = -17.8$ MPa, K_1 is 2, K_2 is 1.9, p_1 is 17.8 MPa, p_2 is 16 MPa, a_1 is 10 m, a_2 is 30 m, a_3 is 10 m, a_4 is 30 m, a_5 is 10 m, a_6 is 10 m, and a_7 is 40 m. Substituting these parameters into Equations ((3)–(5)) enables calculations of the additional stress at any point of the floor of the penta coal seam with the advance of the working face. As the working face advances, the additional stress at 10 m in front of the working face changes with the vertical distance, as shown in Figure 4. The vertical stress, horizontal stress, and shear stress all decrease gradually as the vertical distance h increases. The horizontal stress and shear stress decrease sharply, while the vertical stress decreases slowly. The stresses at 10, 20, and 30 m are 14.25, 9.687, and 7.62 MPa, respectively, and the stress concentration coefficients are 1.8, 1.54, and 1.42, respectively. The additional stress values at 10, 20, and 30 m are 5.767, 3.132, and 1.7 MPa, respectively, and the stress concentration coefficients are 1.32, 1.176, and 1.096, respectively. The shear stress also gradually returns to the original rock stress as the distance increases, indicating that the influential ranges of the horizontal and shear stresses are small. However, the influential range of the vertical stress is larger and decreases rapidly within a certain depth range. When the depth exceeds 30 m, the vertical stress is the mainly contribution to the stress, and the value of the vertical additional stress is close to 0 at 90 m below the

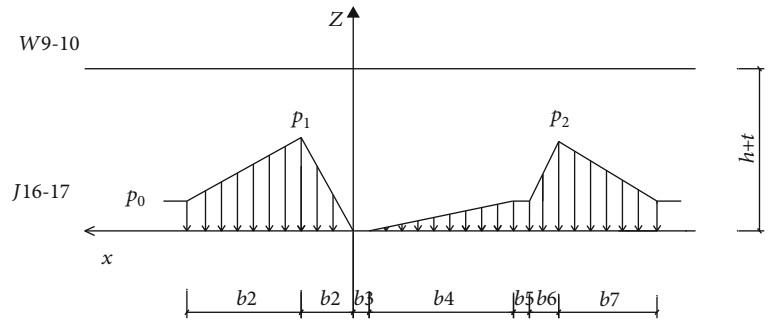

Figure 5: Distribution diagram of roof stress after mining in J coal seam.

floor. Therefore, the influential range of the vertical additional stress on the floor after mining is within 90 m.

2.3. Stress Distribution Law of Overburden in the J Coal Seam of the No. 5 Coal Mine. After the J coal seam is mined, the surrounding rock stress of the mining space is redistributed, and the rock between the W coal seam of the No. 6 mine and the J coal seam of the No. 5 mine is analyzed to evaluate the stress state. After the coal seam is mined, the stress state of this region is depicted in Figure 5.

Here, p_0 is the vertical original rock stress, with a value of $\gamma(h+t)$; p_1 is the peak value of the front abutment pressure, such that $p_1 = k_1 p_0$; p_2 is the peak value of rear abutment pressure, such that $p_2 = k_2 p_0$; b_1 is the distance between the lead pressure peak point and the front coal wall; b_2 is the spacing between the leading pressure peak point and the stress, which has dropped to that of the original rock; b_3 is the distance in the goaf where the original rock stress is zero; b_4 spans the area where the residual pressure is restored to the original rock stress spacing; b_5 is the distance to return to the original rock stress; b_6 is the distance between the peak value of the fixed abutment pressure and the open cut; b_7 is the distance between the peak pressure and the stress that has dropped to that of the original rock.

The linear equation describing the roof stress of the J coal seam can be obtained from Figure 5.

$$q(x) = \begin{cases} \dfrac{p_1}{b_1}x & x \in (0, b_1) \\ \dfrac{p_0 - p_1}{b_2}x + \dfrac{p_1(b_1 + b_2) - p_0 b_1}{b_2} & x \in (b_1, b_1 + b_2) \\ -\dfrac{p_0}{b_4}x - \dfrac{p_0 b_3}{b_4} & x \in (-b_3 - b_4, -b_3) \\ p_0 & x \in (-b_3 - b_4 - b_5, -b_3 - b_4) \\ \dfrac{p_0 - p_2}{b_6}x + \left[p_0 - \dfrac{(p_2 - p_0)(b_3 + b_4 + b_5)}{b_6}\right] & x \in (-b_3 - b_4 - b_5 - b_6, -b_3 - b_4 - b_5) \\ \dfrac{p_2 - p_0}{b_7}x + \left[p_2 + \dfrac{(p_2 - p_0)(b_3 + b_4 + b_5 + b_6)}{b_7}\right] & x \in (-b_3 - b_4 - b_5 - b_6 - b_7, -b_3 - b_4 - b_5 - b_6) \end{cases}. \quad (6)$$

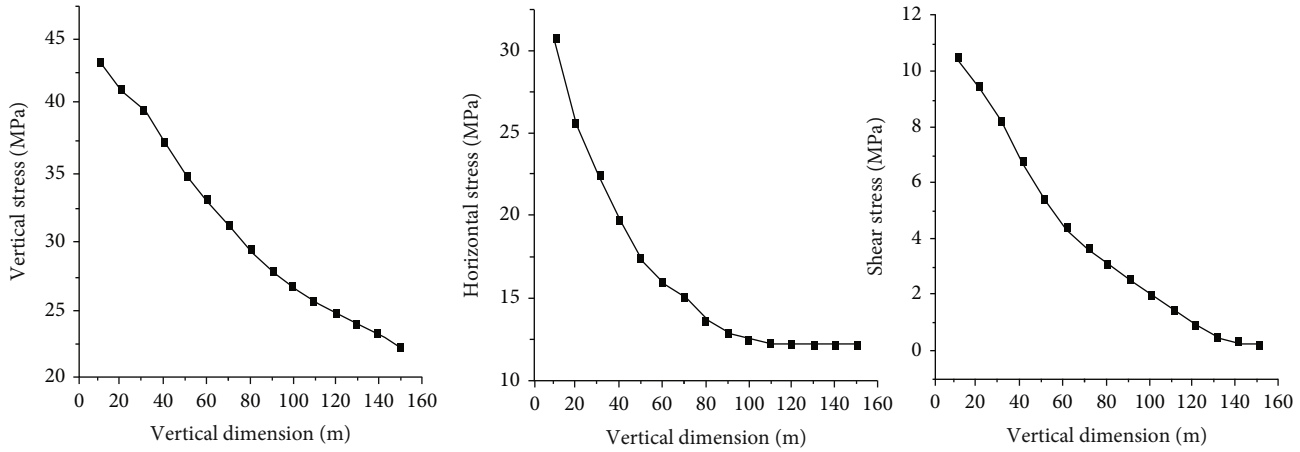

Figure 6: Variations in the roof stress as a function of the distance of the J coal seam.

Table 1: Rock distribution and its physical parameters.

Serial no.	Rock	Thickness (m)	Capacity(kg/m$^{3)}$	Compressive strength (MPa)	Extension (MPa)
31	Medium-grained sandstone	16	2580	70.0	3.5
30	Sandy mudstone	8	2560	21.3	1.5
29	Mudstone	16	2500	21.3	1.8
28	Sandy mudstone	8	2560	21.3	1.5
27	Fine-grained sandstone	4	2600	84.3	4.3
26	Sandy mudstone	10	2560	21.3	1.5
25	Fine-grained sandstone	2	2600	84.3	4.3
24	Mudstone	8	2500	21.3	1.8
23	Sandy mudstone	8	2560	21.3	1.5
22	Fine-grained sandstone	2	2600	84.3	4.3
21	Mudstone	8	2500	21.3	1.8
20	Sandy mudstone	12	2560	21.3	1.5
19	W coal	4	1380	8.66	1.7
18	Sandy mudstone	6	2560	21.3	1.5
17	Mudstone	4	2500	21.3	1.8
16	Siltstone	2	2500	53.8	1.96
15	Sandy mudstone	12	2560	21.3	1.5
14	Mudstone	8	2500	21.3	1.8
13	Fine sandstone	8	2600	84.3	4.3
12	Siltstone	20	2500	53.8	1.96
11	Mudstone	24	2500	21.3	1.8
10	Medium-grained sandstone	16	2580	70.0	3.5
9	Sandy mudstone	20	2560	21.3	1.5
8	Medium-grained sandstone	16	2580	70.0	3.5
7	Sandy mudstone	12	2560	21.3	1.5
6	Fine sandstone	4	2600	84.3	4.3
5	Sandy mudstone	6	2560	21.3	1.5
4	J coal	5	1380	8.66	1.7
3	Mudstone	12	2500	21.3	1.8
2	Fine-grained sandstone	4	2600	84.3	4.3
1	Mudstone	24	2500	21.3	1.8

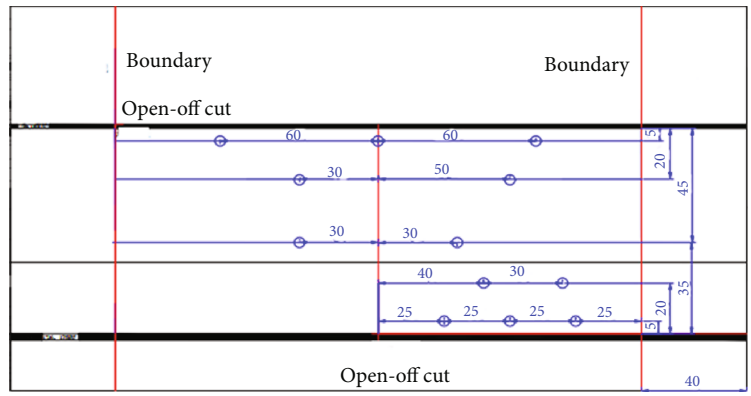

Figure 7: Arrangement of measuring points.

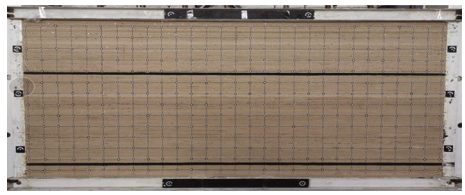

Figure 8: Schematic diagram of the similar material model.

According to Equations (1) and (6), the stress can be determined at a given point in the study area as the working face of the coal seam advances. The expressions for the horizontal stress, shear stress, and vertical stress are shown as

$$\sigma_{x_2} = \frac{2}{\pi}\int_{-b_3-b_4-b_5-b_6}^{-b_3-b_4-b_5-b_6-b_7}\left\{\frac{p_2-p_0}{b_7}x+\left[p_2+\frac{(p_2-p_0)(b_3+b_4+b_5+b_6)}{b_7}\right]\right\}\cdot\frac{z(x-\xi)^2}{\left[(x-\xi)^2+z^2\right]^2}d\xi+\frac{2}{\pi}\int_{-b_3-b_4-b_5-b_6}^{-b_3-b_4-b_5}\left\{\frac{p_0-p_2}{b_6}x+\left[p_0-\frac{(p_2-p_0)(b_3+b_4+b_5)}{b_6}\right]\right\}\cdot\frac{z(x-\xi)^2}{\left[(x-\xi)^2+z^2\right]^2}d\xi+\frac{2}{\pi}\int_{-b_3-b_4-b_5}^{-b_3-b_4}p_0\frac{z(x-\xi)^2}{\left[(x-\xi)^2+z^2\right]^2}d\xi+\frac{2}{\pi}\int_{-b_3-b_4}^{-b_3}-\frac{p_0(x+b_3)}{b_4}\frac{z(x-\xi)^2}{\left[(x-\xi)^2+z^2\right]^2}d\xi+\frac{2}{\pi}\int_0^{b_1}\frac{p_1}{b_1}x\frac{z(x-\xi)^2}{\left[(x-\xi)^2+z^2\right]^2}d\xi+\frac{2}{\pi}\int_{b_1}^{b_1+b_2}\left[\frac{p_0-p_1}{b_2}x+\frac{p_1(b_1+b_2)-p_0b_1}{b_2}\right]\frac{z(x-\xi)^2}{\left[(x-\xi)^2+z^2\right]^2}d\xi, \tag{7}$$

$$\tau_{xz_2} = \frac{2}{\pi}\int_{-b_3-b_4-b_5-b_6}^{-b_3-b_4-b_5-b_6-b_7}\left\{\frac{p_2-p_0}{b_7}x+\left[p_2+\frac{(p_2-p_0)(b_3+b_4+b_5+b_6)}{b_7}\right]\right\}\cdot\frac{z^2(x-\xi)}{\left[(x-\xi)^2+z^2\right]^2}d\xi+\frac{2}{\pi}\int_{-b_3-b_4-b_5-b_6}^{-b_3-b_4-b_5}\left\{\frac{p_0-p_2}{b_6}x+\left[p_0-\frac{(p_2-p_0)(b_3+b_4+b_5)}{b_6}\right]\right\}\cdot\frac{z^2(x-\xi)}{\left[(x-\xi)^2+z^2\right]^2}d\xi+\frac{2}{\pi}\int_{-b_3-b_4-b_5}^{-b_3-b_4}p_0\frac{z^2(x-\xi)}{\left[(x-\xi)^2+z^2\right]^2}d\xi+\frac{2}{\pi}\int_{-b_3-b_4}^{-b_3}-\frac{p_0(x+b_3)}{b_4}\frac{z^2(x-\xi)}{\left[(x-\xi)^2+z^2\right]^2}d\xi+\frac{2}{\pi}\int_0^{b_1}\frac{p_1}{b_1}x\frac{z^2(x-\xi)}{\left[(x-\xi)^2+z^2\right]^2}d\xi+\frac{2}{\pi}\int_{b_1}^{b_1+b_2}\left[\frac{p_0-p_1}{b_2}x+\frac{p_1(b_1+b_2)-p_0b_1}{b_2}\right]\frac{z^2(x-\xi)}{\left[(x-\xi)^2+z^2\right]^2}d\xi, \tag{8}$$

$$\sigma_{z_2} = \frac{2}{\pi}\int_{-b_3-b_4-b_5-b_6}^{-b_3-b_4-b_5-b_6-b_7}\left\{\frac{p_2-p_0}{b_7}x+\left[p_2+\frac{(p_2-p_0)(b_3+b_4+b_5+b_6)}{b_7}\right]\right\}\cdot\frac{z^3}{\left[(x-\xi)^2+z^2\right]^2}d\xi+\frac{2}{\pi}\int_{-b_3-b_4-b_5-b_6}^{-b_3-b_4-b_5}\left\{\frac{p_0-p_2}{b_6}x+\left[p_0-\frac{(p_2-p_0)(b_3+b_4+b_5)}{b_6}\right]\right\}\cdot\frac{z^3}{\left[(x-\xi)^2+z^2\right]^2}d\xi+\frac{2}{\pi}\int_{-b_3-b_4-b_5}^{-b_3-b_4}p_0\frac{z^3}{\left[(x-\xi)^2+z^2\right]^2}d\xi+\frac{2}{\pi}\int_{-b_3-b_4}^{-b_3}-\frac{p_0(x+b_3)}{b_4}\frac{z^3}{\left[(x-\xi)^2+z^2\right]^2}d\xi+\frac{2}{\pi}\int_0^{b_1}\frac{p_1}{b_1}x\frac{z^3}{\left[(x-\xi)^2+z^2\right]^2}d\xi+\frac{2}{\pi}\int_{b_1}^{b_1+b_2}\left[\frac{p_0-p_1}{b_2}x+\frac{p_1(b_1+b_2)-p_0b_1}{b_2}\right]\frac{z^3}{\left[(x-\xi)^2+z^2\right]^2}d\xi. \tag{9}$$

According to the field mining situation and geological environment, the average bulk density of the overburden γ is 0.025 MPa, the mining depth of the W coal seam in the No. 6 mine is 714 m, p is 17.8 MPa, and the coal seam of group J is located 160 m below the coal seam of group W, i.e., $t = 160$ m; thus, the coal seam stress of group J is $p_0 = \gamma(h+t) = 21.85$ MPa, K_1 is 2, K_2 is 1.9, p_1 is 43.7 MPa, p_2 is 41.5 MPa, b_1 is 10 m, b_2 is 50 m, b_4 is 190 m, b_5 is 0 m, b_6 is 10 m, and b_7 is 40 m. By subbing these parameters into the above equations, the stress at any point of the overlying strata after mining can be obtained, and the changes in the peak stress in the upper region can be determined as a function of the vertical distance under the disturbance of mining, as shown in Figure 6.

The vertical stress, horizontal stress, and shear stress gradually decrease as the distance increases. The vertical stress at 10, 30, 80, 120, and 150 m along the roof direction are 43.32, 39.284, 28.503, 24.797, and 23.286 MPa, respectively, and the stress concentration coefficients are 1.98, 1.80, 1.31, 1.13, and 1.064, respectively. The horizontal stress at 10 m is 31.652 MPa, and the stress concentration coefficient is 1.45; the stress at 30 m is 22.653 MPa, and the stress concentration coefficient is 1.034. The shear stress at 10 m is only 0.432 times that of the original rock. These results show that the horizontal stress decreases rapidly as the distance increases, the vertical stress reduction coefficient is slow, and the range of the effects of horizontal stress and shear stress range is small. Moreover, the influence of the vertical stress is relatively larger, indicating that distance mainly

Table 2: Survey line layout positions.

Line	Line no. (from left-to-right)	Distance from top of coal seam (cm)	Remarks
A	A1-A29	2.5	
B	B1-B29	12.5	
C	C1-C29	22.5	
D	D1-D29	32.5	Upper J coal seam
E	E1-E29	42.5	
F	F1-F29	52.5	
G	G1-G29	62.5	
H	H1-H29	72.5	
I	I1-I29	0.5	
J	J1-J29	10.5	
K	K1-K29	11.5	Upper W coal seam
L	L1-L29	12.5	
M	M1-M29	13.5	

affects vertical stress. The stress at 150 m is still greater than the original rock stress, thus clarifying the impact scope of the W coal seam floor in the No. 6 coal mine.

3. Analogous Material Simulations of Mining in a Stubble Coal Seam

3.1. Establishing a Simulation Model. According to the columnar chart of rock strata, the physical and mechanical properties of rock mass, and the size of the similar material simulation frame ($2.85 \times 0.3 \times 2$ m), and considering the principle of similar material simulation tests, the similarity ratios were defined as 1 : 200, 1 : 1.7, 1 : 340, and 1 : 14. The specific strata distribution is shown in Table 1.

The main equipment used in these simulation tests involving similar materials is the model test bed, which includes three systems: model frame system, test system, and loading system. The frame system is a plane stress model test bench ($2.85 \times 0.3 \times 2$ m). The loading system is used to simulate the stope with mining depths above 714 m. The observations can be obtained using a direct measurement method, pressure sensor continuous monitoring, or an XJTUDP measurement system. The XJTUDP measurement system includes a fixed focal length of a high-resolution digital camera, with ID-coded mark points, a ruler, and software dongles, computers, etc.

3.2. Layout of Model Monitoring Points. To study the propagation and distribution law of mining-induced stress in the roof and floor, the stress monitoring points are arranged as shown in Figure 7, i.e., five rows of 12 pressure sensors are arranged in the rock layer of the roof and floor of the coal seam. The distance between the first row and the right boundary is 25 cm. The sensors are numbered 1–3 from right-to-left, and they are 5 cm away from the roof of the coal seam. The distance between the second row and the right boundary is 30 cm, and the pressure sensors are numbered 4–5 from right-to-left, 20 cm away from the roof of coal seam. The third row is 70 cm away from the right boundary, and the pressure sensors are numbered 6–7 from right-to-left, 45 cm away from the floor of the coal seam. The fourth row is 50 cm away from the right boundary, and the pressure sensors are numbered 8–9 from right-to-left, 20 cm away from the floor of the coal seam. The fifth row is 40 cm away from the right boundary, and the pressure sensors are numbered 10–12 from right-to-left, 5 cm away from the floor of the coal seam. The pressure sensors apply the static strain testing system of multiple measuring points to measure the stress changes in each rock layer during mining.

For the automatic continuous monitoring of the monitoring point layout, 406 marking points were distributed on the model in a 10×10-cm grid (the ruler was fixed under the model platform), and six coding marking points were symmetrically fixed on the left and right ends of the test platform, as shown in Figure 8 and Table 2.

3.3. Experimental Steps

(1) Excavation of open cut eyes

Excavation was carried out 40 cm away from the left edge of the model as an open cut for working face mining.

(2) The following data should be recorded after each excavation step:

(a) The length of each excavation: The actual daily feed rate of coal seam mining is 4 m. Based on a temporal similarity ratio of 1 : 14 and a geometric similarity ratio of 1 : 200, the mining work with a coal cutting depth of 2 cm every 1.7 h (actual 24 h) is carried out, which is comparable to the distance of the actual working face advance of 1 day

(b) The falling value of each displacement point by taking pictures at different angles with a digital camera

(c) The height of overlying rock collapse

(d) The stress value of each measurement point obtained by YJZ-32A intelligent digital strain gauge

(3) The model at this point is photographed with a digital camera and imported into the XJTUDP point measurement software for processing to make the corresponding displacement map

3.4. Analysis of Experimental Results

3.4.1. Strata Caving Characteristics. First, the characteristics of the overlying rock caving in the W coal seam were analyzed. Figure 9 shows the overlying rock caving and fracture development during mining in the No. 6 mine's W coal working face. (1) When the working face advances to 32 m, the initial caving phenomenon begins in the direct roof. The caving height reaches 2 m, and the initial caving step

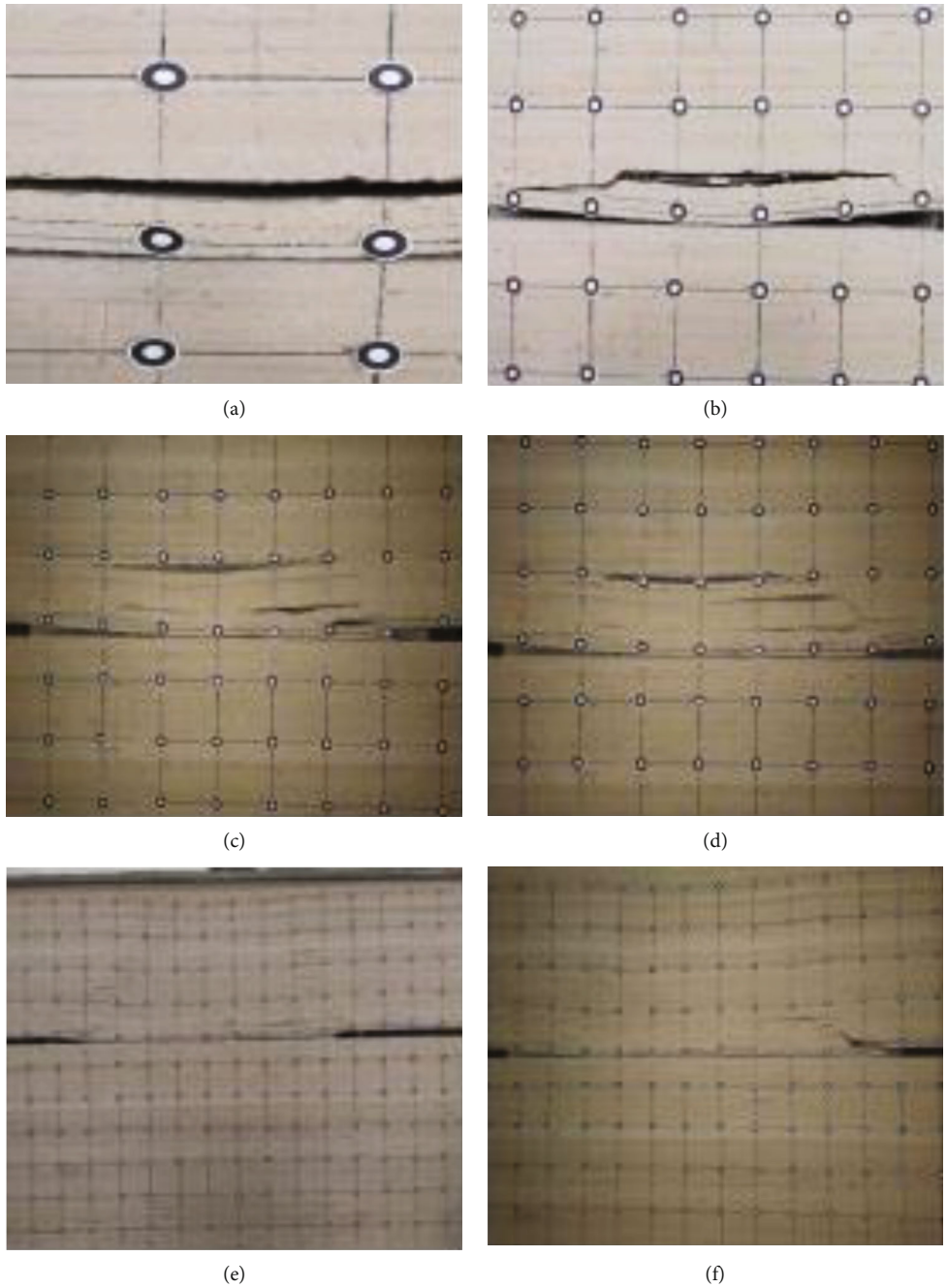

(a) (b) (c) (d) (e) (f)

Figure 9: Continued.

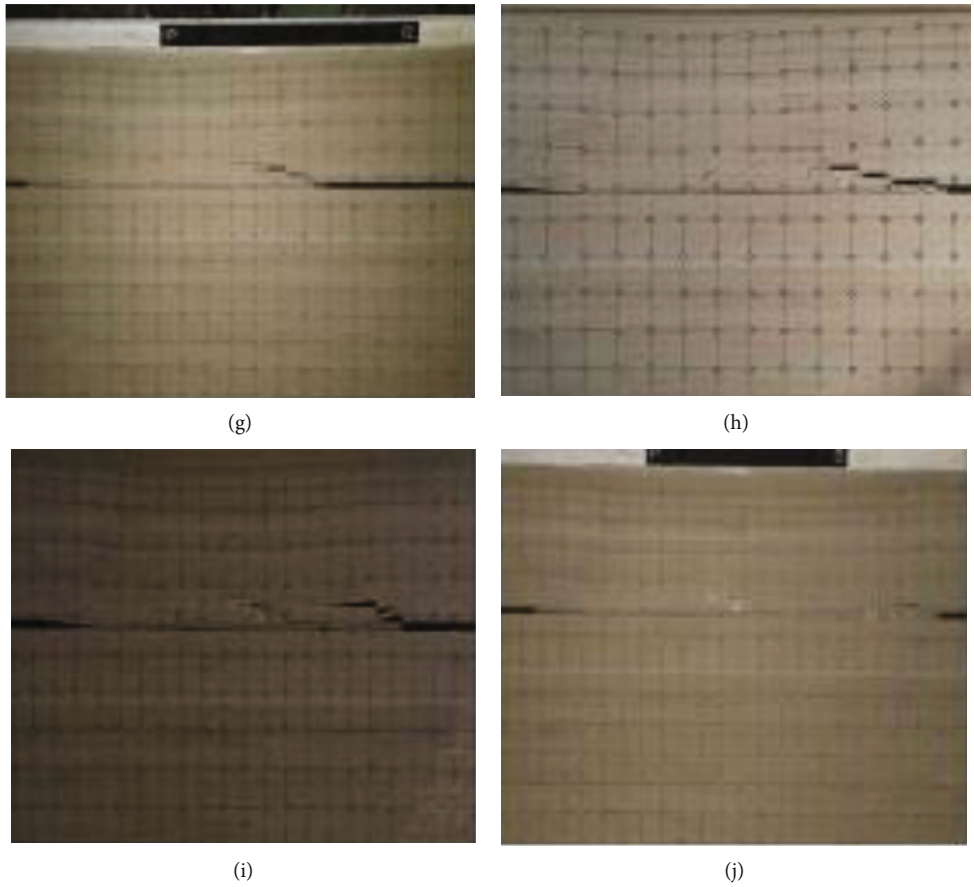

Figure 9: Caving and fracture development of the surrounding rock in the W coal mine as the working face advances to (a) 32 m, (b) 52 m, (c) 68 m, (d) 78 m, (e) 98 m, (f) 110 m, (g) 118 m, (h) 128 m, (i) 168 m, or (j) 200 m.

distance is 32 m. When the working face advances to 52 m, the basic roof strata begin to fracture, and bed-separation cracks appear in the upper goaf roof (approximately 10 m from the height of the roof). As the distance of the working face increases, the rock strata above the basic roof exhibit periodic fracture phenomena. The periodic pressure step distance of the working face is approximately 12–20 m, and the pressure periodicity is clear. (2) During the mining of the $W_{9\text{-}10}$ coal seam, the upper caving strata adopt an arched caving state, and the boundary is composed of the fracture line at the end of the rock beam and the separation fracture line. As the working face advances, the caving strata and the separation strata in the arch gradually extend and expand to the upper and front regions, which causes the periodic failure of the caving arch in the overlying rock. (2) During mining at the $W_{9\text{-}10}$ working face, a caving zone, fracture zone, and bending subsidence zone are formed successively in the overlying strata of the goaf from bottom-to-top. The height of the caving zone is ~10 m, which is about 2.5 times the mining height. The resulting fracture zone height is ~51 m, which is 12.8 times the mining height.

Second, the characteristics of the overlying rock caving in the J coal seam were evaluated. The working face of the J coal seam is 160 m below the working face of the W coal seam in the No. 6 coal mine. The length of the stubble mining area is 100 m. Figure 10 shows the development of stope rock caving and fracture during fully mechanized mining in the J coal seam. It should be noted that when the working face of $W_{9\text{-}10}$ is reaching 200 m, the working face of $J_{16\text{-}17}$ in the stubble area will be mined after it has stabilized. During the mining process, the strata caving and fracture development in the stope have the following characteristics. (1) When the working face of the J coal seam is reaching 42 m, the direct roof of the coal seam will experience the first caving phenomenon, and the height of the caving rock layer is 3 m. When pushed up to 68 m, bed-separation fractures appear in the interbedded strata, and the primary fracture in the basic roof strata is induced. As the working face continues to advance, the direct roof at the upper part of the coal seam gradually falls forward, and the failure and deformation of the overburden continuously develop and extend upward toward the front. At this point, the average periodic underloading step distance is approximately 12 m, and the periodic underloading phenomenon is clearer. (2) As the $J_{16\text{-}17}$ working face advances, there is an arched caving state in the rock strata in the stubble area. As the advancing distance increases, the caving rock strata in the arch extend and expand upward and forward, and the final size of the caving arch is smaller than that of the caving arch formed when the W coal seam in the No. 6 coal mine is pushed to the same distance. The reason for this phenomenon is that the pressure is reduced because of the mining of the W coal

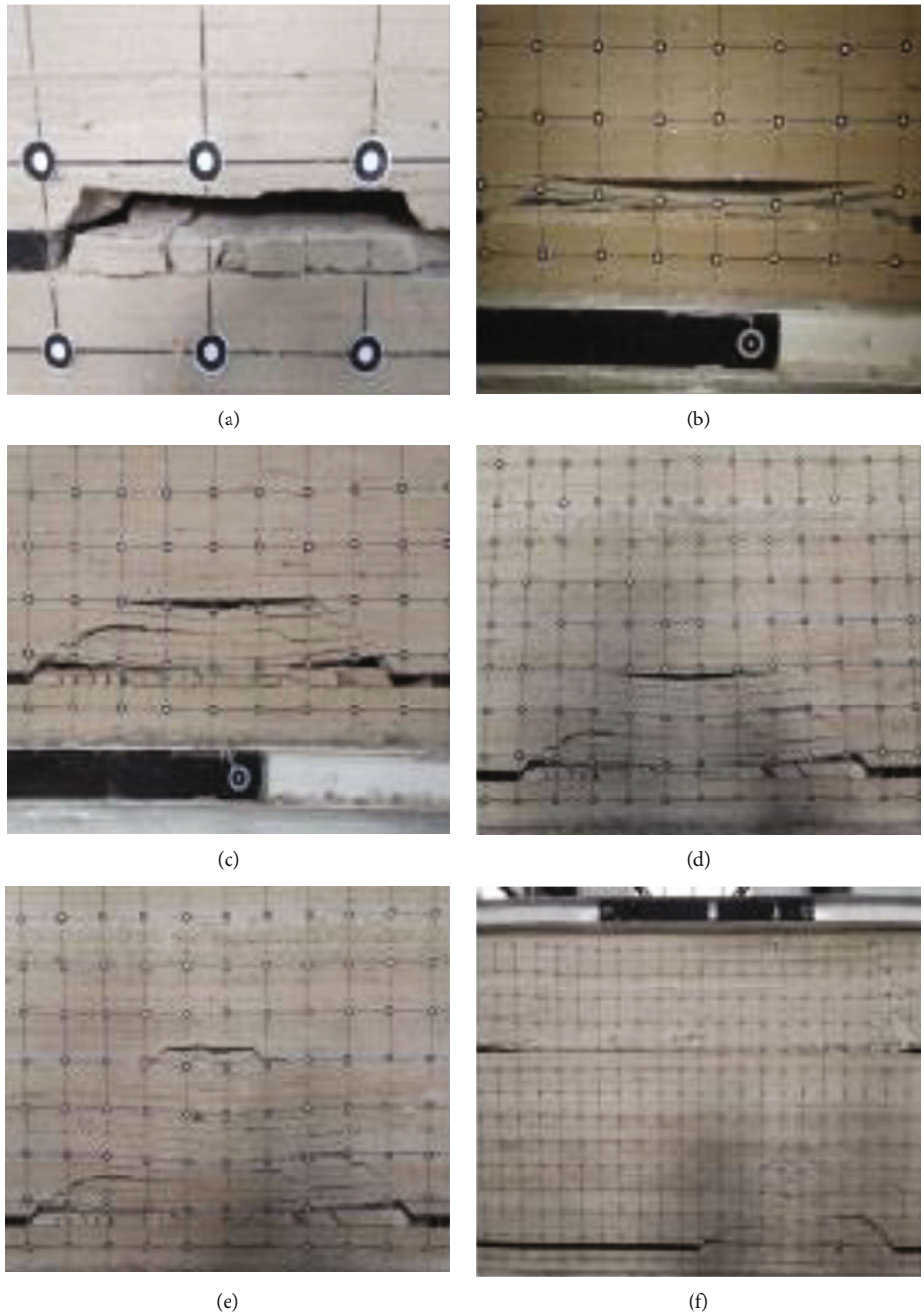

Figure 10: Caving and fracture development of surrounding rock in the J coal seam as the working face is pushed to (a) 42 m, (b) 68 m, (c) 82 m, (d) 92 m, (e) 100 m (bureau), and (f) 100 m (whole).

seam in the No. 6 coal mine at the upper part of the stubble area. (3) The goaf in the stubble of the $J_{16\text{-}17}$ coal seam of the No. 5 coal mine and the $W_{9\text{-}10}$ coal seam of the No. 6 coal mine did not break through. The working face of the $W_{9\text{-}10}$ coal seam is located in the bending subsidence zone of the working face of the $J_{16\text{-}17}$ coal seam. Comparing the final caving states of the rock strata in Figure 10(f) and Figure 9(j) reveals that the mining of the $J_{16\text{-}17}$ coal seam in the lower part of the stubble area promotes the caving of the $W_{9\text{-}10}$ coal seam in the upper part of the stubble area and the development of fractures in the coal wall of the working face, as well as the overall transfer to the stubble area. The reason for this phenomenon is that with the gradual filling and compaction of the rock strata above the goaf at the $J_{16\text{-}17}$ coal seam in the lower part of the stubble area, the displacement and fracture of the rock strata above the upper $W_{9\text{-}10}$ coal seam continue to develop under the overall pressure. These observations indicate that the goaf of the two mines is not penetrated under the stubble pressure environment; however, with the mining of the lower part of the $J_{16\text{-}17}$ coal seam

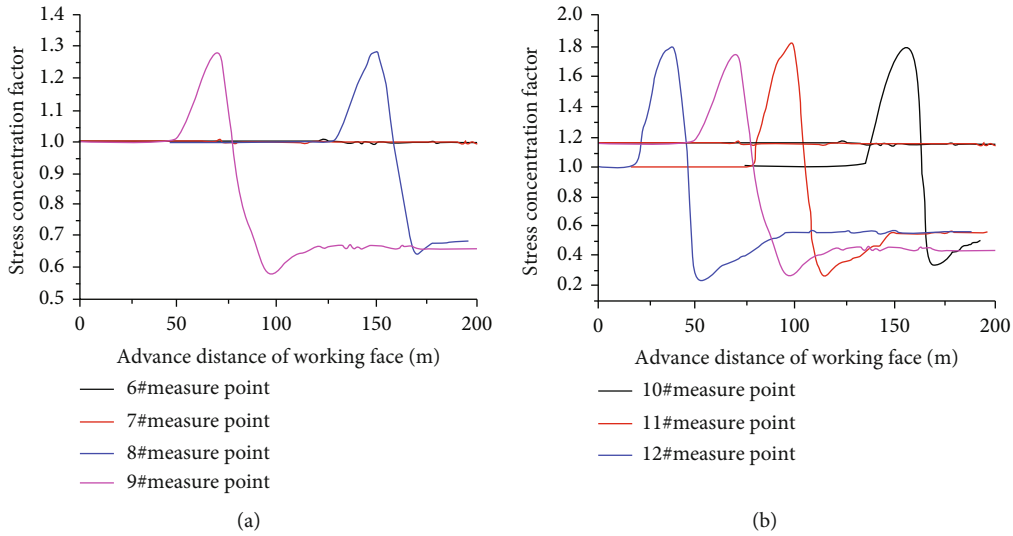

Figure 11: Stress concentration coefficient curves of each mining point in the W coal seam.

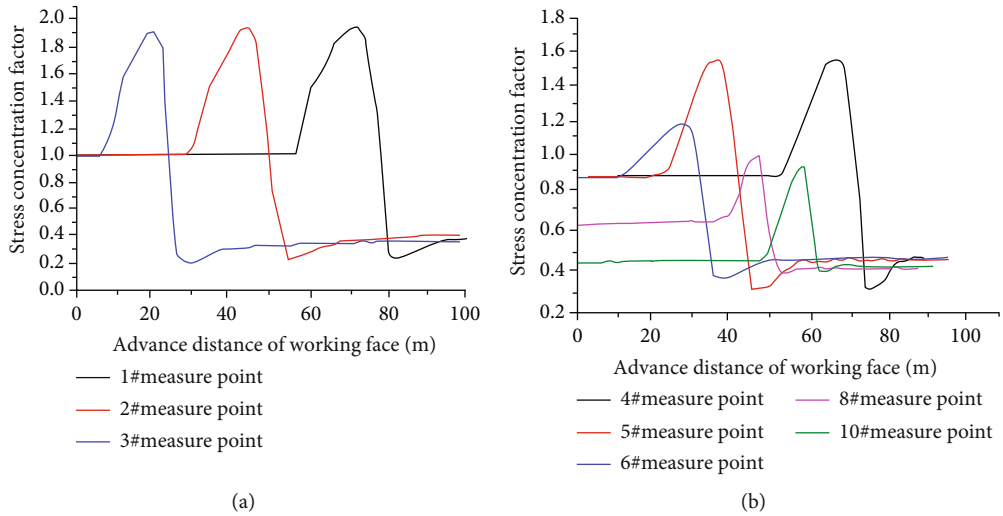

Figure 12: Stress concentration coefficients at mining points in the J coal seam.

working face, the development and range of overlying rock fractures in the $W_{9\text{-}10}$ coal seam will gradually continue to increase.

3.4.2. Changes in the Mining Stress. As the working face advances, various phenomena (e.g., caving, bed-separation, bending, and subsiding) occur in the overlying strata of the goaf, and floor heave occurs in the floor, all of which can change the stress in the rock mass around the stope. To establish the dynamic law governing the roof and floor stresses during coal mining, the stress concentration factor (i.e., the ratio of the real time stress to the initial stress of the coal seam) is determined. According to the relationship between the excavation distance of the working face and the change in the stress values at each pressure measuring point in the rock layer, the stress propagation distribution laws along the roof and floor of the coal seam can be obtained as a function of the advancing distances, as shown in Figures 11 and 12 for the W and J coal seams, respectively.

Figure 11 illustrates the mining-induced stresses in the W coal seam; the horizontal coordinate is the working face advance distance, and the vertical coordinate is the stress concentration coefficients. As the working face advances in the W coal seam of the No. 6 coal mine, the stress concentration coefficients at each pressure measuring point in the rock layer (from 6 to 12) were obtained, thus revealing changes in the stress state of the roof and floor and redistribution of the stress. Therefore, according to the stress distribution, the roof and floor areas can be divided into five regions. The first region comprises the area not affected by mining: (i) the area far from the working face (because at a greater distance, this part of the rock is less affected by coal mining, so it maintains the original rock stress state) and (ii) the area 40–50 m outside. The second region is the increased stress area:

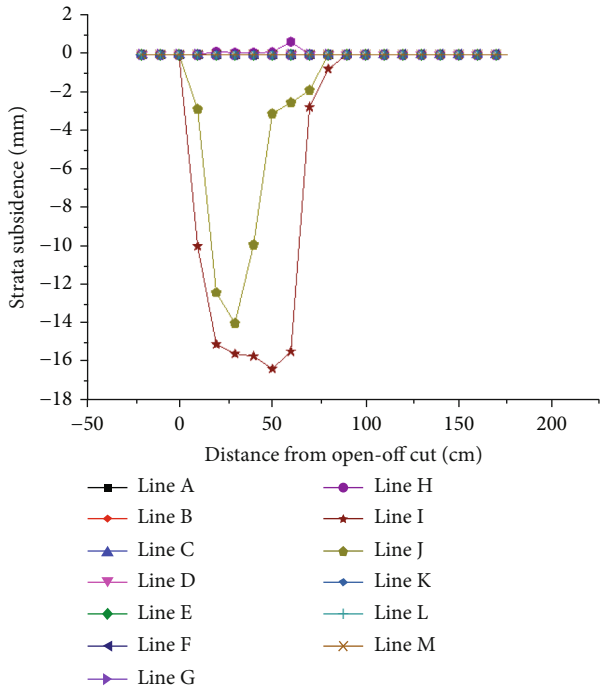

Figure 13: Displacement curve when the W coal working face is pushed 80 m.

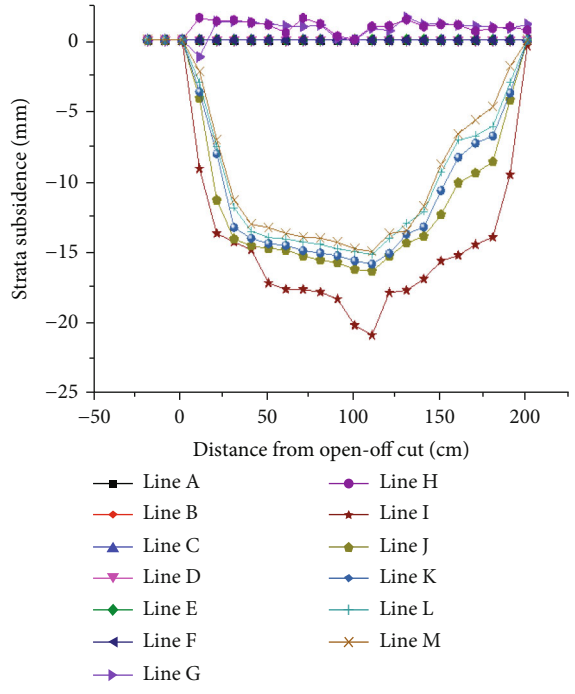

Figure 14: Displacement curves when the working face is pushed 200 m.

this area is intensely affected by mining, i.e., 2–40 m in front of the working face (the position of the stress peak moves with the advance of the working face, and the average distance from the working face is ~10 m). The third region includes the stress reduction area: this region is located in the goaf, where the overlying rock caving phenomenon

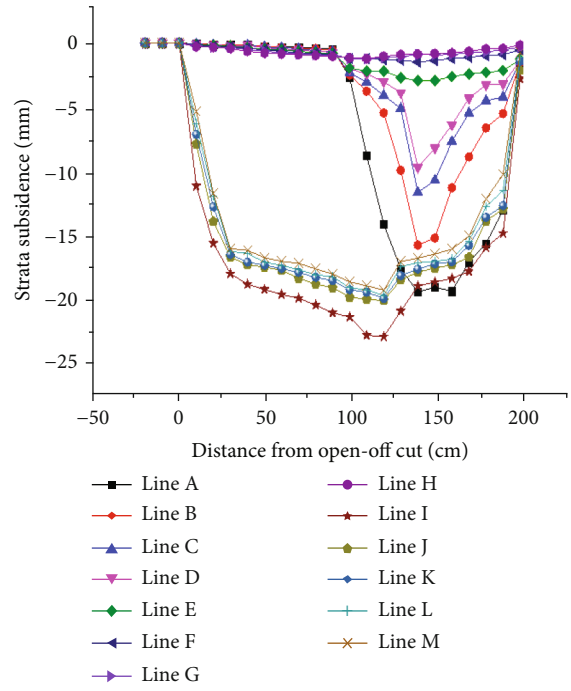

Figure 15: Displacement curve of the J coal working face advanced to 100 m.

occurs. As the pressure is transferred to the caving gangue and the surrounding coal and rock mass, this area is located within 2–20 m behind the working face. The fourth region is the pressure growth area: because the goaf is gradually filled and compacted, the stress in the caving rock begins to recover to some extent. This area is behind the working face within approximately 10–40 m. The fifth region is the stress stability area: based on the advanced distance of the working face, the caved gangue is gradually compacted, and the stress finally tends to stabilize. This area is located at the rear of the working face, approximately 25–40 m away from the open cut.

During the mining of the W coal seam of the No. 6 coal mine, as the working face advances, the stress concentration coefficient changes according to the distance under the floor. After the working face advances, the surrounding rock stress of the floor stope is redistributed. As the advancing distance increases, the maximum stress concentration coefficient in front of the working face also gradually increases, although the rate of increase slows and it ultimately reaches a stable state. In general, the stress concentration coefficients of measuring points at different positions under the floor decreases as the vertical distance increases, and the distance between the position of the stress peak and the coal wall also increases. A vertical distance of 45 m from the W coal seam floor (#6 stress curve) corresponds to the site of faults in the pressure area, W coal seam mining for floor 6# points where layers of location had no effect. Because of the similar material simulation experiment with a geometric similarity ratio of 1 : 200, it is possible to model the W coal seam of the No. 6 coal mine's impact on the bottom plate within a depth of 90 m.

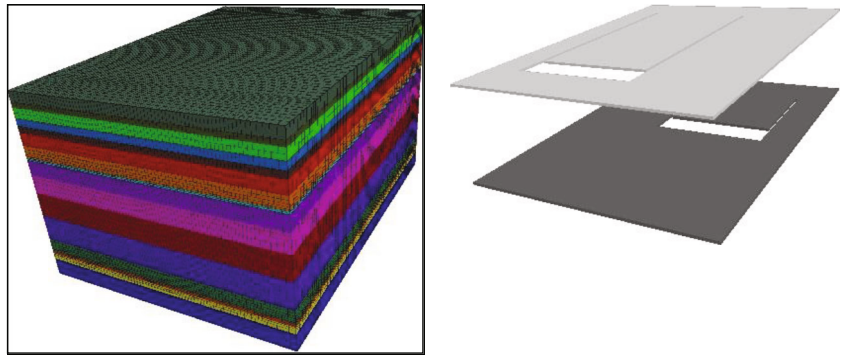

(a) (b)

Figure 16: Computational diagrams of (a) the 3D model and (b) coal seam excavation.

Table 3: Rock distribution and physical parameters.

Rock	Density (kg.m^{-3})	Elasticity modulus (GPa)	Poisson's ratio	Cohesion (MPa)	Frictional angle (°)	Extension (MPa)
Medium-grained sandstone	2580	20.23	0.21	12.3	35.01	3.5
Sandy mudstone	2570	27.28	0.24	2.32	40.39	3.6
Mudstone	2570	26.35	0.23	2.03	41	1.8
Sandy mudstone	2570	27.28	0.24	2.32	40.39	3.6
Fine-grained sandstone	2600	22.31	0.33	14.32	36.32	4.3
Mudstone	2500	26.35	0.23	2.03	41	1.8
Sandy mudstone	2570	27.28	0.24	2.32	40.39	3.6
W coal	1350	3.57	0.26	0.77	40.24	1.5
Sandy mudstone	2570	27.28	0.24	2.32	40.39	3.6
Fine-grained sandstone	2600	22.31	0.33	14.32	36.32	4.3
Mudstone	2500	26.35	0.23	2.03	41	1.8
Medium-grained sandstone	2580	20.23	0.21	12.3	35.01	3.5
Sandy mudstone	2570	27.28	0.24	2.32	40.39	3.6
J coal	1350	3.57	0.26	0.77	40.24	1.5
Mudstone	2500	26.35	0.23	2.03	41	1.8
Fine-grained sandstone	2600	22.31	0.33	14.32	36.32	4.3

Analogously, the variation law of mining stress in the J coal seam was evaluated. Owing to the mining influence of the working face of the W coal seam in the No. 6 coal mine, the floor strata in a certain range induced a certain pressure relief effect, and the coal seam pressure was reduced compared with the conditions involving a single mine. Figure 12 shows the variations in the vertical stress of the mining roof overburden on the working face of the J coal seam of the No. 5 coal mine in the stubble area. These data revealed the following characteristics. (1) According to the curve derived from stress measuring points 1–3, the stress concentration of the measuring points along the same horizontal line increases as the working face advances, while the influential range of stress also increases. (2) From the curve derived from pressure measuring points 4–6, the stress concentration coefficient decreases gradually with increasing vertical distance from the working face, which indicates that the farther away from the working face, the weaker the influence of coal mining. (3) During working face mining, as the vertical distance between stress measuring points in different strata and the working face increases, the effect of vertical stress on the roof and floor of the stope is gradually weakened; however, the pressure relief in the rock strata along the same horizontal survey line remains unchanged by the forward mining of the working face. (4) According to stress measuring points 8 and 10, mining at the working face of the J coal seam in the No. 5 coal mine produces secondary stress concentration phenomena at the roof. Therefore, mining at the working face of the J coal seam in the No. 5 coal mine has a significant impact on the roof, thereby inducing stress concentration on the floor of the W coal seam in the No. 6 coal mine. However, the supporting pressure caused by

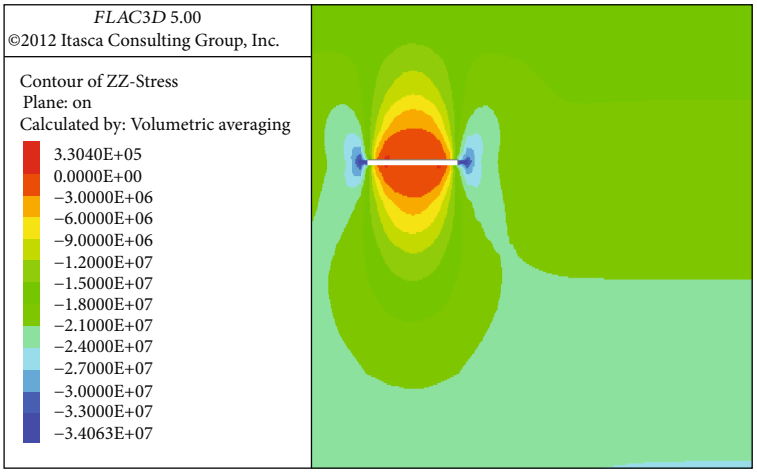

(a)

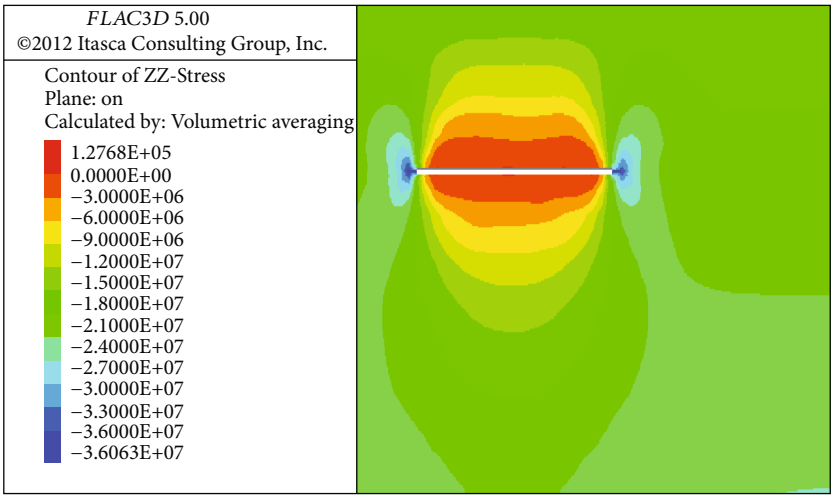

(b)

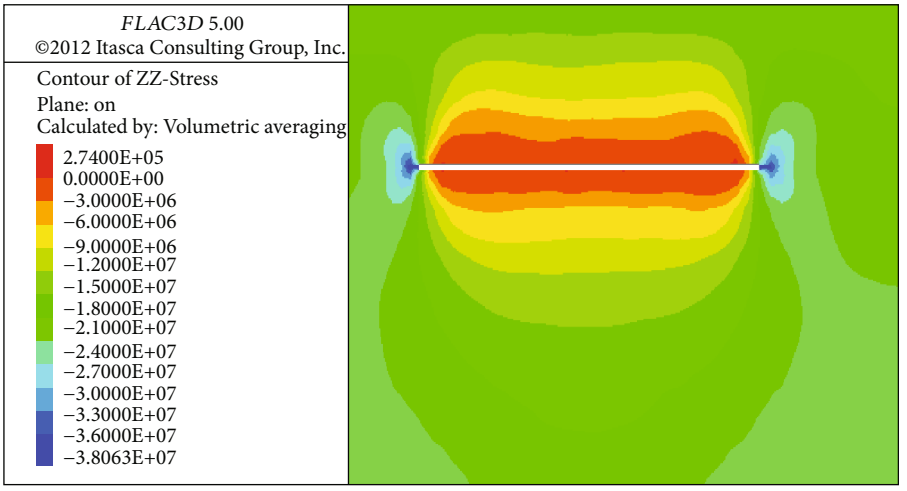

(c)

Figure 17: Continued.

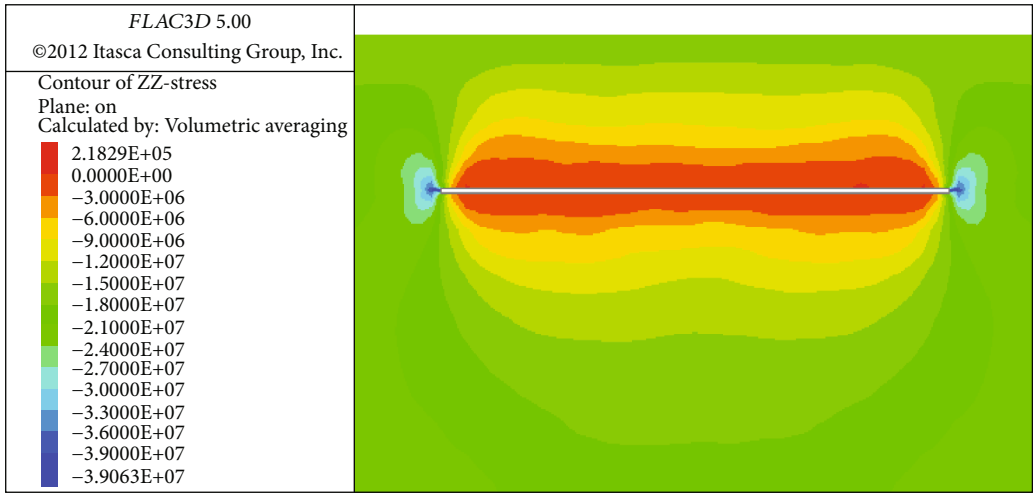

(d)

Figure 17: Vertical stress distribution of propulsion in the W coal seam as the working face is pushed to (a) 100 m, (b) 200 m, (c) 300 m, and (d) 400 m.

mining at the working face of the W coal seam in the No. 6 coal mine is less than that of the J coal seam in the No. 5 coal mine, and the influential range is consistent with the analytical mining stress results.

3.4.3. Displacement Variation Law. In the similar material simulation, the working face mining occurs in forward distance steps of 4 m to monitor changes in strata displacement caused by advancing after stabilization. A camera was used to photograph and record the model to clearly and visually depict the effect of displacement changes after mining. Then, the effect of displacement during working face advancement can be analyzed. This experiment was analyzed under three advancing conditions (80 and 200 m for the W coal seam and 100 m for the J coal seam); the displacement curves for the roof and floor strata during simulated working face advancement are presented in Figures 13–15, respectively.

It is clear from Figure 13 that when the working face advances forward to 80 m (to the coal seam roof of I), the J line displacement changes significantly, whereas the rest of the strain measurement lines exhibit no appreciable changes. The face behind the mined-out area in the surface displacement of the roof and floor rock masses change. In general, two similar lines will change; in this case, the roof line changed because I is close to the excavation site of the coal seam; therefore, the influence of mining is most severe for the I line, followed by the J survey line. Analyzing the H, I, and J displacement lines indicated that the working face advancement gradually changes, and the maximum deformation of rock strata displacement along the H displacement line experienced a swelling up phenomena, although the effect is small. Meanwhile, the I and J lines gradually sank, achieving maximum subsidence in 25 to 50 locations. These results show that as the working face advances, the bottom floor heaves, and the roof strata cave in. The maximum subsidence was reached in the middle of the goaf.

Figure 14 shows that the displacement of the surrounding rock of the stope changes significantly with the advance of the working face. Specifically, as the working face advances, the overall in a given displacement measuring line is similar to the case where the working face of the W coal seam is advanced to 200 m. Compared with the displacement changes to the surrounding rock of the roof and floor in the goaf when it is pushed to 80 m, the roof collapse and floor bulging phenomena were enhanced significantly. The closer the vertical distance to the coal seam, the more obvious the effect of mining, and the greater the maximum displacement settlement and uplift. At this point, the maximum settlement of survey line I has clearly reached the mining height of the coal seam, indicating that the overlying rock collapse phenomenon has induced compaction at a position of 100 m (in the middle of the coal seam), while the displacement of lines J–M (above) decreases gradually according to the distance from the working face, although maximum subsidence is observed at approximately 100 m (in the middle of the goaf). Considering the uncompacted position of the goaf overburden, the corresponding floor bulging phenomenon also emerges.

It is clear from Figure 15 that as the working face of the J coal seam advances under stubble pressure at the bottom of the No. 6 mine, the displacement curves of roof A–D subside significantly, followed by the other displacement measurement lines, and the maximum displacement in all cases was in the middle and front of the goaf. The survey line of the goaf and the upper roof strata in the No. 6 coal mine continues to increase, and the position of the maximum displacement is transferred to the side of the stubble area. The change of displacement measurement lines after mining of the coal seams of No. 5 coal mine and No. 6 coal mine indicates that in the stubble environment, the mining of the J coal seam of No. 5 coal mine will shift the overall pressure above the roof of the W coal seam of No. 6 coal mine to the stubble zone, resulting in the downward movement of the overburden of the W coal seam of No. 6 coal mine and the disturbance effect of shifting to the stubble zone.

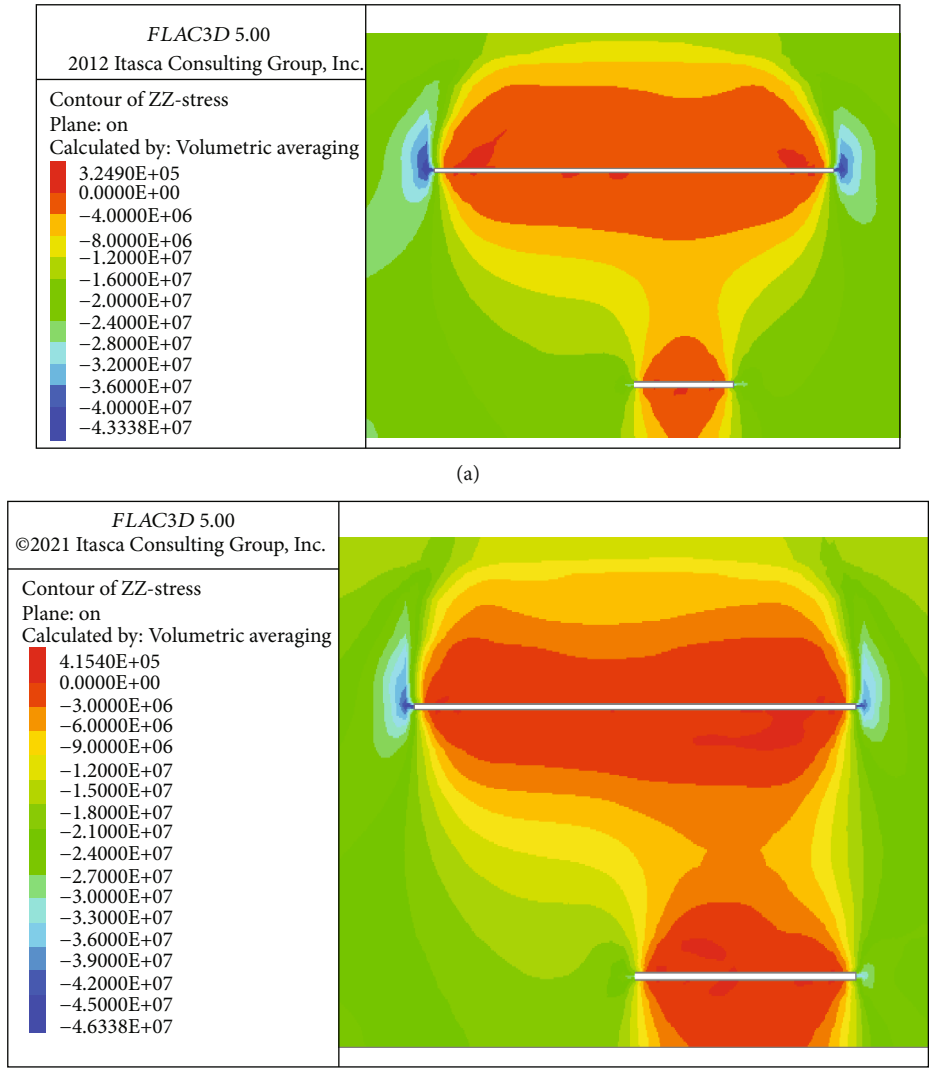

Figure 18: Vertical stress distribution of propulsion in the J coal seam as the working face is pushed to (a) 100 m, (b) 200 m.

4. Numerical Simulation of the Influence of Coal Seam Mining in the Stubble Area

4.1. Model Establishment and Calculation. The FLAC3D numerical simulation software was used to simulate the mining of the coal seam, and the laws of coal and rock stress fields were analyzed in terms of the advancing working face. The calculation model was established according to the bar chart, i.e., the length, width, and height of the model were 560, 400, and 309 m, respectively. The Moor-Coulomb model was adopted as the constitutive model for these numerical calculations. The obtained three-dimensional model is shown in Figure 16(a), and the excavation of the coal seam is illustrated in Figure 16(b). The excavation interval length of the W coal seam was 80–480 m, and that of the J coal seam was 280–480 m. The physical and mechanical properties of the rock formation in the model are shown in Table 3.

4.2. Influence of Coal Mining. To obtain the W coal seam in the No. 6 coal mine and the J coal seam in the No. 5 coal mine, the pressure crop area between the two mines' coal seams must be simulated with an appropriate environment. Specifically, the W and J coal seam working face excavation simulations and the stress changes were evaluated to study the rock damage; however, the experiment failed to reflect the roadway surrounding rock deformation.

4.2.1. Stress Distribution. Figure 17 shows the changes in the vertical stress distribution as the working face advanced during the mining of the W coal seam in the No. 6 coal mine. When advancing to 100 m, the stress of the roof and floor of the goaf and both ends of the working face change, the stress gradient of the roof and floor decrease in the pressure relief state, and the stress concentration phenomenon occurs at both ends of the working face. When the advancement distance increases to 200 m, the pressure relief range of goaf

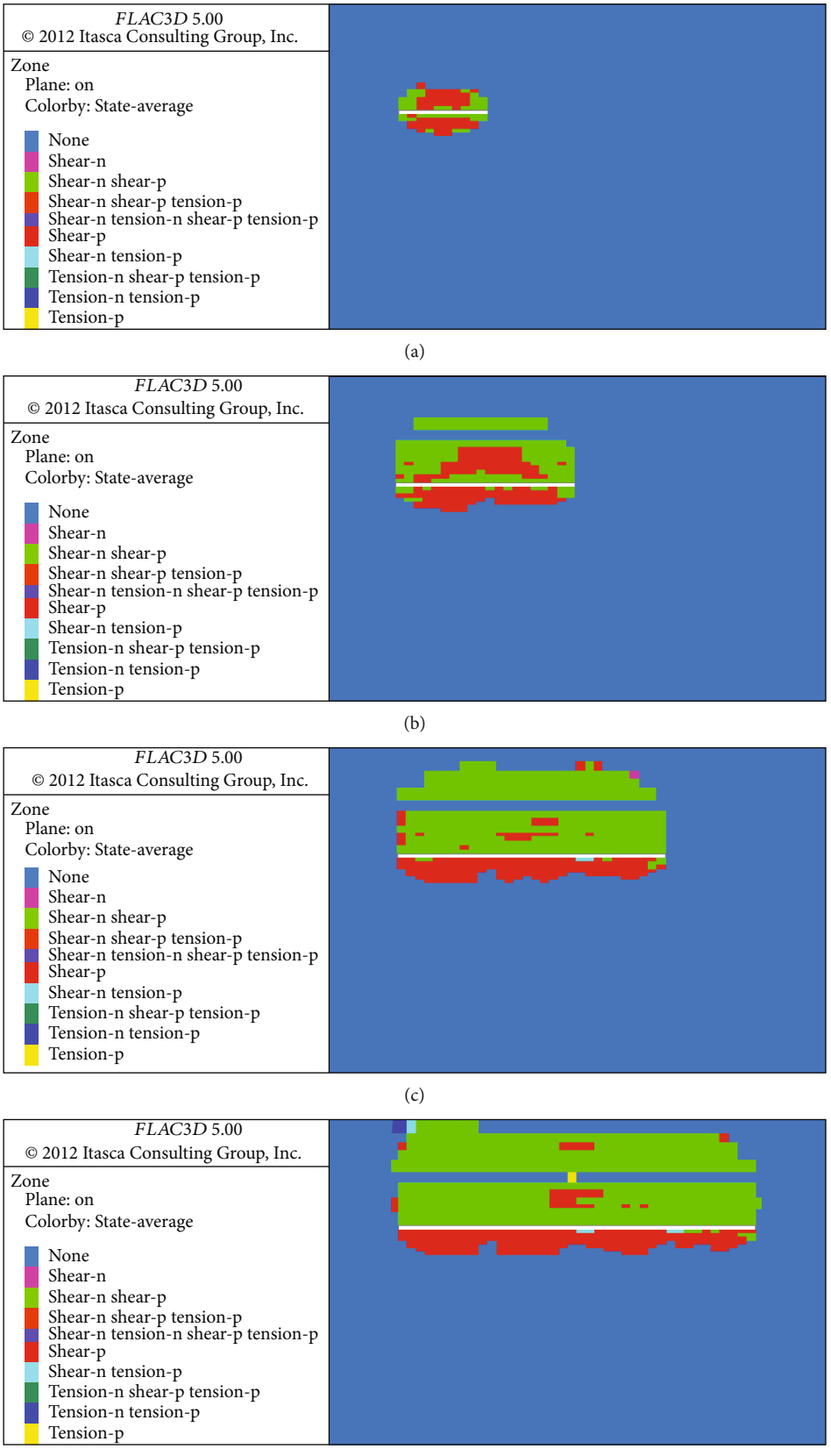

Figure 19: Cloud diagrams of the plastic zone changes in the propulsion of the W coal seam when the working face is pushed to (a) 100 m, (b) 200 m, (c) 300 m, and (d) 400 m.

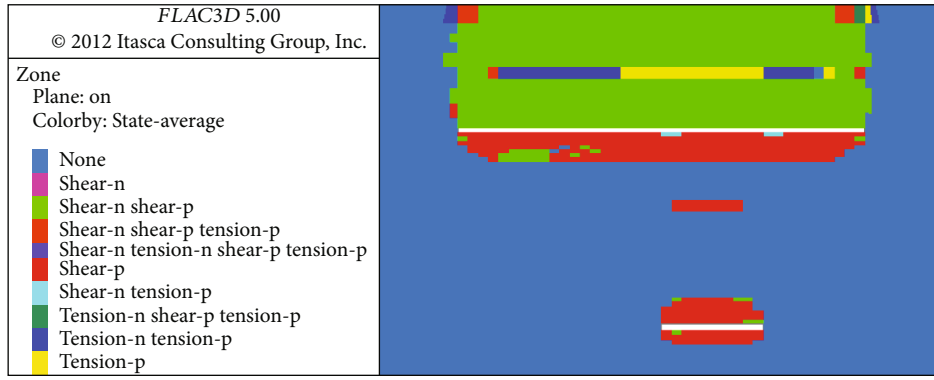

(a)

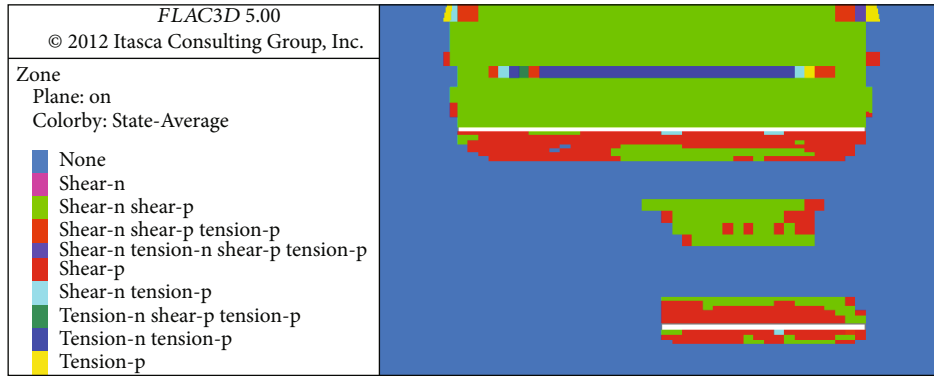

(b)

Figure 20: Cloud diagrams of the plastic zone changes in the propulsion of the J coal seam when the working face is pushed to (a) 100 m and (b) 200 m.

increases significantly in the depth and length directions. Simultaneously, a stress reduction area is established in the region from 10 m behind the mining face to 10 m before the cutting face, and the stress concentrations at both ends also increase. When the advancement distance is 300 m, the relief area continues to grow; when the advancement distance is 400 m, the relief area increases significantly in the depth direction, indicating that the rear caving rock layer is gradually compacted as the working face advances.

Figure 18 shows that when the J coal seam in the No. 5 coal mine (located in the stubble part of the lower part of the W coal seam in the No. 6 coal mine) is mined to 100 m, stress changes occur in the coal seam surrounding rock. Specifically, the stress concentration phenomenon emerges in the W coal seam in the No. 6 coal mine, the roof and floor stress state decrease with increasing advancement distance, and up and down mining and coal unloading occur when advancing to 200 m. As a result, the stress concentrations at the coal seam ends of the two mines gradually increase, and the stress concentration is generally more obvious. As the pressure relief area grows, the pressure reduction area in the stubble area also increases substantially.

4.2.2. Variation of the Plastic Zone. Figure 19 presents the distribution cloud map of the plastic zone as a function of the working face advancement during the mining of the W coal seam in the No. 6 coal mine. When the working face is advanced to 100 m, the roof and floor of the goaf formed by coal seam excavation are subjected to shear and tensile forces, and the failure area is formed. The rock strata collapse, cracks appear, and the roof failure height is ~20 m. This situation is entirely consistent with the height of rock strata collapse and crack development observed in the experiments. The failure depth of the bottom plate is approximately 18 m. When the pushing distance increases, the range of the plastic zone increases along the length and height directions. When the pushing distance reaches 400 m, the maximum damage height of the plastic zone in the roof reaches 100 m, and the damage depth of the floor reaches 20 m.

Figure 20 shows that when the J coal seam in the No. 5 coal mine is mined in the stubble area at the lower part of the W coal seam in the No. 6 coal mine, as the working face advances and the pressure increases, the crop area clearly increases the range of the plastic zone. Moreover, the W coal seam floor in the No. 6 coal mine exhibits significant damage depth, and the J coal seam in the No. 5 coal mine has clear damage at the height of the roof. At this point, the failure range and failure mode of the roof and floor of the W coal seam in the No. 6 coal mine change. The failure depth of the floor of the stubble area increases to 24 m. In the stubble area (except for the failure area of the floor of the W coal seam), the maximum failure area is 92 m away from the roof of the J coal seam in the No. 5 coal mine. This can explain

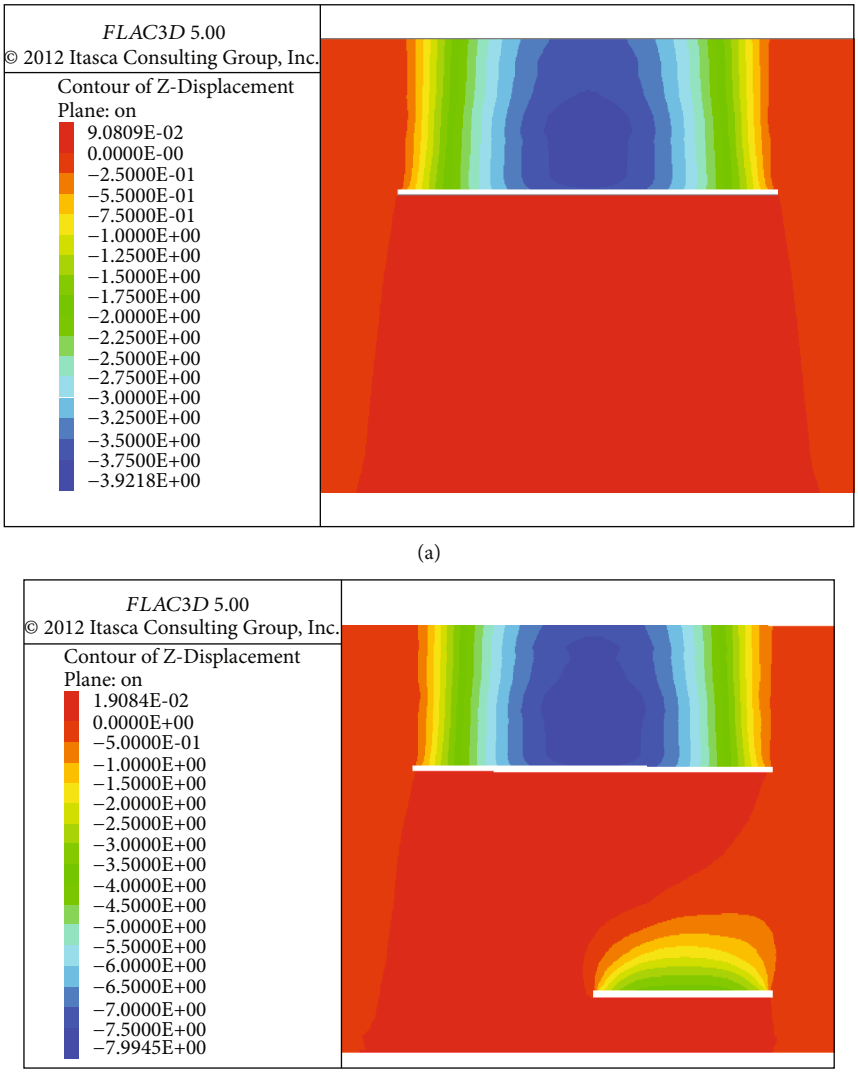

Figure 21: Displacement cloud diagrams of the mining of the (a) W coal seam in the No. 6 coal mine and (b) J coal seam in the No. 5 coal mine.

why the W coal seam and the J coal seam have two mining pressure crop relations: only mining the W coal seam in the No. 6 coal mine affects its roof and floor, whereas mining the J coal seam in the No. 6 coal mine not only affects its own roof and floor, but can also still generate a pressure crop area while the damage to the W coal seam roof and floor continues to increase.

4.2.3. Variations in the Displacement Field. It is clear from Figure 21 that the displacement field changes due to the mining of the W coal seam in the No. 6 coal mine. The maximum displacement of the roof is 3.93 m, which is similar to the mining height of the coal seam (4.0 m), and floor heaving occurs. At this point, there is no influence on the roadway of the J coal seam in the No. 5 coal mine in the stubble area. When the J coal seam in the No. 5 coal mine is being mined, the maximum displacement above the roof is 4.7 m, which is similar to the mining height (5.0 m); this result indicates that the displacement of this model is consistent with the experimental model, which verifies the accuracy of the simulations. However, because the mining of the J coal seam in the No. 5 coal mine affects the displacement of the rock strata in the stubble area, it induces a secondary disturbance effect on the displacement of the upper part of the W coal seam in the No. 6 coal mine. This leads to a change in the overall displacement and ultimately affects the roadway of the W coal seam in the No. 6 coal mine.

According to the above analysis, the mining of the overlying W coal seam in the No. 6 coal mine does not affect the roadway of the J coal seam in the No. 5 coal mine of the underlying stubble area. In fact, the roadway of the J coal seam is only affected by its own mining, whereas the roadway in front of the working face of the W coal seam is not only affected by its own mining, but also by the secondary mining of the underlying J coal seam.

5. Conclusions

Based on the theory of elasticity, a stress field computational model of the overlying and underlying working face of stubble coal seams was established. Considering the geological engineering conditions, similar material simulation experiments and numerical simulations were applied to elucidate the variations in vertical stress, horizontal stress, and shear stress at the top and bottom (i.e., as a function of the vertical distance). Additionally, the changes in overburden caving, stress and displacement, and the influential range of coal mining in a stubble environment were analyzed, leading to the following conclusions:

(1) During the mining of the $W_{9\text{-}10}$ working face, the initial pressure stepping distance caused by the mining of the working face is 32 m, and the periodic pressure stepping distance is 12–20 m. The overlying strata of the goaf form a caving zone, fracture zone, and bending subsidence zone successively from bottom-to-top. The height of the caving zone is ~10 m (about 2.5 times the mining height); the resulting fracture zone height is ~51 m (12.8 times the mining height). When the $J_{16\text{-}17}$ working face is mined, the initial pressure step distance caused by mining is 42 m, the periodic pressure step distance is 8–16 m, and the average periodic pressure step distance is 12 m. The working face of the $W_{9\text{-}10}$ coal seam is located in the bending subsidence zone of the working face of the $J_{16\text{-}17}$ coal seam. As the working face of the $J_{16\text{-}17}$ coal seam advances, the development and range of overburden rock fractures of the $W_{9\text{-}10}$ coal seam gradually increase

(2) For the stubble area of the No. 5 and No. 6 coal mines, the changes in the stress and displacement caused by the advancing progress of the working face were obtained. The support pressure and displacement caused by the mining process of the No. 6 coal mine have no appreciable effect on the stubble seam of the No. 5 coal mine. However, the mining of the $J_{16\text{-}17}$ coal seam of the No. 5 mine leads to an increase in the overburden displacement of the $W_{9\text{-}10}$ coal seam of the No. 6 mine; the maximum displacement is transferred to the rear, and the concentration is more obvious in the middle and front regions of the stubble area. In terms of the coal seam excavation under stubble conditions, the stress concentrations at the roof and floor and the deformation of the surrounding rock continue to increase in the No. 6 coal mine due to the mining of the coal seam in the No. 5 and No. 6 mines, as well as the excavation of the coal seam in the overlying stubble area, which shows the effect of superposition

(3) The coal seam mining stresses in the roof and floor decrease with increasing vertical distance; the distance is the main contributing factor to the vertical stress on the coal seam. Overlying the vertical stress induced by mining only occurs when the working face is within 90 m; however, the influential scope of the stress caused by the underlying working face mining is larger, such that the roadway is still affected at 160 m

(4) By studying the overburden deformation law of adjacent mines under the condition of stubble coal mining, it was possible to obtain the overburden stress distribution, stress changes, displacement changes, and other laws impacting adjacent mines. The results presented herein provide a theoretical basis and technical support for the prevention and control of underground dynamic disasters while offering insights regarding the mining of coal seams in mine groups

6. Prospects

(1) In this paper, we only consider the effect of fixed horizontal stubble distance and different vertical distance of coal seams in two mines on the influence of coal seam mining under stubble conditions on the deformation of roadway surrounding rock, and we should further study the influence of multiple mine seam stubble and different horizontal stubble distance to provide further theoretical basis for the study of underground shaft group

(2) In order to study the deformation law of mining overburden under stubble conditions more precisely, field tests should be conducted to monitor by multiple means, or three-dimensional similar material simulation tests should be conducted for research

Data Availability

Supplemental data that support the summary findings of this study are available from the corresponding author, upon reasonable request.

Conflicts of Interest

The authors have no relevant financial or nonfinancial interests to disclose.

Authors' Contributions

All authors contributed to conceptual design and methodology.

Acknowledgments

This work was financially supported by the National Key Research and Development Program of China (No. 51774173).

References

[1] X. Li, S. Chen, E. Wang, and Z. Li, "Rockburst mechanism in coal rock with structural surface and the microseismic (MS)

and electromagnetic radiation (EMR) response," *Engineering Failure Analysis*, vol. 124, no. 6, article 105396, 2021.

[2] L. M. Dou, X. Y. Tian, A. Y. Cao et al., "Current status and problems of impact ground pressure prevention and control in coal mines in China," *Journal of Coal*, vol. 47, no. 1, pp. 152–171, 2022.

[3] C. J. Fan, S. Li, D. Elsworth, J. Han, and Z. Yang, "Experimental investigation on dynamic strength and energy dissipation characteristics of gas outburst-prone coal," *Energy Science & Engineering*, vol. 8, no. 4, pp. 1015–1028, 2020.

[4] X. L. Li, Z. Y. Cao, and Y. L. Xu, "Characteristics and trends of coal mine safety development," *Energy Sources, Part A: Recovery, Utilization, and Environmental Effects*, pp. 1–14, 2021.

[5] B. X. Jia, L. L. Zhou, Y. S. Pan, and H. Chen, "Artificial seismic source field research on the impact of the number and layout of stations on the microseismic location error of mines," *Advances in Civil Engineering*, vol. 2019, Article ID 1487486, 11 pages, 2019.

[6] N. B. Zhang, Z. H. Ouyang, and L. H. Kong, "Characteristics of strata movement and stress evolution of close distance coal seams mining with hard roof," *Safety in Coal Mines*, vol. 47, no. 1, pp. 216–219, 2016.

[7] Z. Cheng, H. Ma, C. Sang, and Y. Liu, "Experimental research on dynamic evolution characteristics of roof movement and mining-induced stress of superimposed mining in a close distance coal seam group," *Geotechnical & Geological Engineering*, vol. 39, no. 1, pp. 13–24, 2019.

[8] W. B. Guo, M. J. Liu, H. M. Li, and X. L. Shi, "Photoelastic simulation of surrounding rock stress in multi-seam mining," *Acta Coal Sinica*, vol. 1, pp. 8–12, 2001.

[9] W. B. Guo, N. Li, and W. Yk, "Photoelastic simulation study on stress distribution of soft rock roadway," *Acta Coal Sinica*, vol. 6, pp. 596–600, 2002.

[10] R. S. Yang, Y. Zhu, Y. L. Li, and W. Y. Li, "Stress distribution law and damage damage characteristics of roadway bottom slab in laminated rock," *Journal of China University of Mining and Technology*, vol. 49, no. 4, 2020.

[11] Y. W. Shi, "Preliminary study on three-dimensional stress distribution around stope," *Mine Pressure*, vol. 2, pp. 117–122, 1989.

[12] Y. W. Shi, "Principle of bearing force of stope face and rock strata control," *Coal Science and Technology*, vol. 2, 1997.

[13] S. L. Lu, "Selection of horizontal distance X between roadway and upper coal pillar edge," *Journal of China University of Mining and Technology*, vol. 22, no. 2, pp. 1–7, 1993.

[14] S. L. Lu, Y. D. Jiang, and Y. L. Sun, "Selection of vertical distance Z between roadway and upper coal seam," *Journal of China University of Mining and Technology*, vol. 22, no. 1, pp. 1–7, 1993.

[15] X. F. Luo and G. J. Yang, "Research on similar simulation of Qiangjiaying short-range coal seam group mining," *Coal Technology*, vol. 26, no. 1, pp. 52–54, 2007.

[16] B. B. Yang, S. C. Yuan, D. Z. Zheng et al., "Study on the spatial and temporal evolution characteristics of overburden fissures in repetitive mining of close coal seams," *Journal of Mining and Safety Engineering*, pp. 1–9, 2022.

[17] X. Z. Yue, M. Tu, Y. F. Li, J. S. Zhang, and L. Gao, "Calculation of additional stresses of mining in the roadway under the bottom slab of the coal column at the legacy boundary of close coal seam mining," *Journal of Mining and Safety Engineering*, vol. 38, no. 2, 2021.

[18] H. Q. Liu, L. Wang, L. C. Han, P. Liu, and P. Zou, "Study on the instability mechanism and control measures of a roadway in a mine with retained coal pillars and close coal seams," *Shock and Vibration*, vol. 2021, 14 pages, 2021.

[19] H. Q. Liu, "Study on floor roadway stability under the influence of near coal seam mining," *Coal Engineering*, vol. 49, no. 5, pp. 44–46, 2017.

[20] Q. G. Zhao, B. Wang, S. D. Zheng, J. J. Shi, and Y. Y. Liu, "Failure characteristics of surrounding rock of roadway in mining floor of upper coal seam and pressure relief control technology," *Coal Engineering*, vol. 48, no. 8, pp. 77–80, 2016.

[21] W. B. Guo and C. Li, "Impact analysis of remote lower coal seam mining on upper stope roadway," *Journal of Henan Polytechnic University*, vol. 37, no. 2, pp. 22–28, 2008.

[22] Y. X. Zhao, W. H. Liu, C. Zhang et al. , "The evolution of stress and fracture in the surrounding rock of close coal seam stirrup mining," *Journal of Coal*, vol. 47, no. 1, pp. 259–273, 2022.

[23] Z. Zhou, C. Q. Zhu, and Q. F. Li, "Failure mechanism and stability control of surrounding rock of roof roadway in fracture zone," *Journal of Coal*, vol. 42, no. 6, pp. 1400–1407, 2017.

[24] C. J. Hou, X. Y. Wang, J. B. Bo, N. K. Meng, and W. D. Wu., "Study on the basic theory and technology of stability control of deep roadway rock surroundings," *Journal of China University of Mining and Technology*, vol. 50, no. 1, pp. 1–12, 2021.

[25] K. Ding, S. Gu, J. Guo, D. Gu, Z. Liu, and B. Wei, "Numerical Investigation on factors affecting stability of roadway surrounding rock with fractured roof," *Geotechnical and Geological Engineering*, vol. 37, no. 4, 2019.

[26] Z. P. Jin, *Study on Overburden Movement Law and Surrounding Rock Deformation Mechanism in Short-Range Coal Mining in Shaping Mine*, China University of Mining and Technology, Beijing, 2018.

[27] Y. Xing, P. H. S. W. Kulatilake, and L. A. Sandbak, "Effect of rock mass and discontinuity mechanical properties and delayed rock supporting on tunnel stability in an underground mine," *Engineering Geology*, vol. 238, pp. 62–75, 2018.

[28] J. P. Guo, W. G. Wang, F. L. He, and G. C. Zhang, "Analysis of basic top breaking structure and stability of surrounding rock in large section comprehensive discharge along empty roadway," *Journal of Mining and Safety Engineering*, vol. 36, no. 3, 2019.